THE ASTROPHYSICAL JOURNAL, 447:103–120, 1995 July 1

TWO CLASSES OF GAMMA-RAY EMITTING ACTIVE GALACTIC NUCLEI

CHARLES D. DERMER
E. O. Hulburt Center for Space Research, Code 7653, Naval Research Laboratory, Washington, DC 20375-5352;
dermer@osse.nrl.navy.mil

AND

NEIL GEHRELS
Laboratory for High Energy Astrophysics, Goddard Space Flight Center, Greenbelt, MD 20771;
gehrels@lheavx.gsfc.nasa.gov
Received 1994 June 15; accepted 1995 January 13

ABSTRACT

We interpret recent gamma-ray observations of active galactic nuclei (AGNs) made with the Whipple Observatory, *Granat* and especially the *Compton Gamma Ray Observatory*. The gamma-ray data show that there are two distinct classes of AGNs defined by their redshift and luminosity distributions and high-energy spectral properties. Sources in the first class, which are generally associated with AGNs classified in other wavelength ranges as Seyferts, have redshifts $z \lesssim 0.06$ and 50–150 keV luminosities in the range 10^{41}–10^{44} ergs s^{-1}. These sources display spectral softenings at ~ 100 keV energies, with no measured emission at photon energies $E >$ several MeV. This class includes radio-quiet AGNs in addition to radio galaxies apparently viewed at large angles with respect to the radio jet axis. The redshifts of objects in the second class, which are associated with AGNs classified as blazars, are as large as $z \cong 2.3$, and the range of 100 MeV–5 GeV luminosities, assuming isotropic emission, extends to 10^{49} ergs s^{-1}. The ≈ 20 MeV–30 GeV gamma-ray luminosity often dominates the bolometric luminosity in objects of this class. These sources probably represent AGNs that are observed nearly along the axis of a radio jet. Some AGNs show evidence from the high-energy data for transitional behavior between the two classes.

We consider whether the qualitatively different properties of the two gamma-ray classes provide evidence for quasi-isotropic emission from the Seyferts and beamed emission from the blazars. Comparison of the observed redshift and luminosity distributions with model distributions derived from a treatment of the cosmological statistics of isotropic and beamed sources gives, however, inconclusive results. We treat gamma-ray transparency arguments for beaming, avoiding earlier unproven assumptions that X-rays and $E > 100$ MeV gamma rays originate from the same site. The pair-production optical depth of $E > 100$ MeV gamma rays interacting with other gamma rays is much less than 1 and does not require beaming, but data from OSSE give evidence for beaming in a few blazars. We generalize to the gamma-ray regime the Elliot-Shapiro relation, which is based on the assumption that AGN radiation is isotropically emitted and that the luminosity is generated by Eddington-limited accretion. Available gamma-ray data do not yet demonstrate a strong conflict with this limit. The generalization of the Eddington-luminosity limit to the Klein-Nishina limit suggests, however, a new type of object that can accrete at luminosities much greater than $10^{46}\ M_8$ ergs s^{-1} by radiating photons at gamma-ray energies. Here M_8 is the black hole mass in units of $10^8\ M_\odot$. Beaming arguments from gamma-ray observations require more observations of blazars, but superluminal observations probably still provide the most compelling evidence for bulk relativistic motion in blazars.

Subject headings: galaxies: active — galaxies: jets — galaxies: nuclei — galaxies: Seyfert — gamma rays: observations

1. INTRODUCTION

Active galactic nuclei (AGNs) form an observational group defined by the presence of highly luminous and variable emission from the cores of galaxies which remain unresolved even on the milliarcsecond scale. The bolometric luminosities of AGNs, assuming isotropic emission, are in the range 10^{42}–10^{49} ergs s^{-1}, and the power for all types of AGNs is almost universally ascribed to accretion onto supermassive black holes with masses $M \sim 10^6$–$10^9\ M_\odot$. Within the general AGN category, there is a rich diversity of source types identified through observations made in the radio-through-X-ray regimes. These include Seyferts, radio galaxies, BL Lacertae objects (BL Lacs), quasi-stellar objects (QSOs), and quasi-stellar radio sources (quasars). Although each subgroup has markedly different properties, a classification scheme is emerging which organizes many of the AGN types in terms of unifying characteristics related to geometrical orientation and the absence or presence of radio jets (see Lawrence 1987; Bregman 1990; Urry, Maraschi, & Phinney 1991 for reviews). For example, differences in the properties of radio-quiet objects such as Seyfert 1 and 2 AGNs can be largely understood in terms of geometrical obscuration effects (for a recent review, see Antonucci 1993). The presence of radio jets in radio-loud sources provides additional orientation-dependent effects arising from radiation anisotropy, probably due to Doppler boosting (e.g., Begelman, Blandford, & Rees 1984; Dermer & Schlickeiser 1992).

Here we interpret recent gamma-ray data from AGNs obtained with the Whipple Observatory, the *Granat* mission, and especially the *Compton Gamma-Ray Observatory*. From

the standpoint of gamma-ray astronomy, the differences in AGN types were not important until the recent gamma-ray results. Early observations with limited sensitivity (e.g., Bignami et al. 1979; Bassani & Dean 1983) suggested that most AGNs had similar gamma-ray spectra, namely a hard power-law continuum with photon spectral index $s \approx 1.6$ (where the photon flux $\Phi[E]$ [photons cm^{-2} s^{-1} MeV^{-1}] $\propto E^{-s}$) up to ≈ 2 MeV, above which the spectrum steepened to $s \approx 2.5$–3.5. This shape matched the known X-ray spectra at low energies and was supported by the few high-energy data: $E > 100$ keV for NGC 4151 (Perotti et al. 1981a), $E > 700$ keV for Centaurus A (von Ballmoos, Diehl, & Schönfelder 1987), and $E > 100$ MeV for 3C 273 (Swanenburg et al. 1978). This spectral shape was also readily understood as nonthermal emission from accelerated particles near the black hole, with photon-photon pair production (Jelly 1966; Herterich 1974) attenuating the flux at energies much above $m_e c^2$ (Bignami et al. 1979; Lightman & Zdziarski 1987).

The new data from *Compton* show that gamma-ray spectra for different types of AGNs are not, in fact, similar. In this paper, we classify AGNs detected at gamma-ray energies (which we call gamma-ray AGNs) and consider the implications of this classification. (The impact of recent high-energy observations on our theoretical understanding of AGNs has also been recently assessed by Zdziarski 1994 and Marscher & Bloom 1994.) The gamma-ray observations are summarized in § 2. From the hardness ratios and redshift and luminosity distributions of gamma-ray AGNs, we show in § 3 that Seyferts and radio galaxies represent one class of gamma-ray AGNs and blazars a second class. This conclusion is amplified in § 4 by an examination of the high-energy and broadband spectra of objects in each class. We also describe some transitional objects which do not fit clearly into either class. In § 5 we consider evidence for bulk relativistic outflow and beaming on the basis of the redshift and luminosity distributions and the time variability and intensity of the high-energy radiation from gamma-ray AGNs. The cosmological statistics of gamma-ray AGNs do not require beaming, only enormous luminosities, and we demonstrate weaknesses in arguments for relativistic bulk motion and beaming from gamma-ray transparency arguments and the Elliot-Shapiro relation. Weak evidence for variability on timescales of a few days from OSSE observations presently provides the strongest evidence for beaming from the gamma-ray data alone. The implications of the high-energy results on our multiwavelength understanding are discussed in § 6.

2. GAMMA-RAY OBSERVATIONS OF ACTIVE GALACTIC NUCLEI

Table 1 is a list of AGNs that have been positively detected at photon energies $E > 20$ keV.[1] Blank entries mean that there have been no reports of observations in that energy range. The 20–165 keV column refers to *HEAO 1*, *Exosat*, and *Ginga* observations, the 50–150 keV column to OSSE and SIGMA/*Granat* observations, the 1–30 MeV column to the Imaging Compton Telescope (COMPTEL) observations, the $E > 100$ MeV column to EGRET observations, and the $E > 0.5$ TeV column to Whipple Observatory observations although the ultra–high-energy entry for Cen A refers to its unconfirmed detection by Grindlay et al. (1975) at $\gtrsim 0.3$ TeV. Table 1 also lists the measured photon fluxes from the detected sources in the indicated energy ranges in units given by note 3 to Table 1. With much overlap between the different instruments, the detections include (see Table 1 for references): 12 Seyferts and radio galaxies in the *HEAO 1* sample (including Cen A, but omitting Mrk 335 because it was not positively detected at >20 keV with the A2 and A4 instruments on *HEAO 1*); 24 AGNs detected with the OSSE instrument on *Compton* in the range 50–150 keV; five AGNs detected with SIGMA,[2] the hard X-ray/soft gamma-ray telescope on *Granat*; five strong and two marginal detections of AGNs with COMPTEL on *Compton* in the 1–30 MeV energy range; 44 AGNs detected with the EGRET on *Compton* in the medium energy (20 MeV–30 GeV) gamma-ray regime; Mrk 421, detected (Punch et al. 1992) at very high energies ($\sim$400 GeV–2 TeV) with the Whipple Observatory; and numerous AGN observations with balloon instruments. This table is not absolutely complete, since it omits some quasars that were weakly detected with *Ginga* (Ohashi et al. 1989) above 20 keV. It also does not include starburst galaxies such as NGC 253, detected with OSSE (Bhattacharya et al. 1994).

In Table 2, the benchmark operating characteristics of the Whipple Observatory and the gamma-ray telescopes on *Granat* and *Compton* are given for reference. Note that COMPTEL and EGRET have completed full-sky surveys, while the other instruments view only selected sources. Approximate upper limits can be determined from the sensitivity limits give in Table 2 for the entries in Table 1 for which there were no positive detections.

The OSSE team has reported positive detections (Johnson et al. 1994; Kurfess 1994) of 24 AGNs as shown in Table 1. Four nondetections of AGNs with the OSSE instrument are also noted in Table 1, and additional nondetections have been reported elsewhere (Cameron et al. 1993; McNaron-Brown et al. 1995). Some objects have been positively detected during one viewing period but not during another, suggesting variability. Of the OSSE-detected AGNs, 12 are classified as Seyfert 1's, five are Seyfert 2's (including NGC 4151), and the remaining seven include five quasars and two BL Lac objects. Three of the Seyfert 1's and one of the Seyfert 2's are also radio galaxies. By extrapolating *HEAO 1* and *Ginga* spectral data for Seyfert 1 galaxies into the OSSE energy range, many more and stronger detections of AGNs were expected than have been observed. The implication is that the spectra of Seyfert 1 nuclei soften considerably when going from the hard X-ray to the soft gamma-ray regimes. The magnitude of this softening for the average Seyfert spectrum, excluding the brightest ones, has been quantified by Johnson et al. (1994). They find a mean OSSE Seyfert spectral index of $\langle s_\gamma \rangle = 2.20 \pm 0.15$ in the range 50–150 keV, steeper by ≈ 0.5 units than the canonical 2–10 keV spectral index $\langle s_X \rangle \cong 1.70 \pm 0.17$ measured with *EXOSAT* (Turner & Pounds 1989). It is important, however, to take into account a reflection component (Zdziarski et al. 1995) in order to precisely quantify the extent of spectral softening.

No Seyfert AGNs or radio galaxies have been reported as sources of $E > 1$ MeV radiation (Schönfelder 1994; Lin et al.

[1] See Malaguti, Bassani, & Caroli (1994) for a catalog of AGN observations at $E \geq 0.01$ keV through the end of 1992.

[2] The AGNs detected with SIGMA are NGC 4151, NGC 4388, 3C 273, Cen A, and 1E 1227+0224 (Paul 1994; Jourdain et al. 1992b). Only 1E 1227+0224 was not positively detected with OSSE because of its proximity of 15′ to 3C 273.

TABLE 1

ACTIVE GALACTIC NUCLEI DETECTED AT >20 keV

Source	Type	z	20–165 keV	50–150 keV	1–30 MeV	>100 MeV	>0.5 TeV	Reference
NGC 4151	Sy 1.5–2	0.0033	Y: 3.4–10.	Y: 15.–31.	N	N: <0.05	N	1–24
NGC 7582	Sy 2	0.0049		Y: 2.6–5.1	N			19, 21, 22
NGC 6814	Sy 1	0.0053	Y: 2.6	Y: 3.2	N			8, 19, 22, 25
MCG −6−30−15	Sy 1	0.0078		Y: 4.0–5.0	N	N: <0.1		19–23
MCG −5−23−16	Sy 2	0.0082	Y: 3.3	Y: 4.0–4.9				8, 21–22
NGC 4388	Sy 2	0.0087		Y: 6.4				21, 25, 26
NGC 3783	Sy 1	0.0092	Y: 0.8	Y(3 σ): ~4	N	N: <0.12		8, 18, 19–22
IC 4329A	Sy 1	0.0157		Y: 4.2–5.9	N	N		18, 19, 21, 22, 27–29
NGC 5548	Sy 1	0.017	Y: 0.6	Y(3 σ): 3.3–4.7	N	N		8, 19–23, 30, 31
MCG +8−11−11	Sy 1	0.0205	Y: ~8.0	Y: 2.2–4.0	N	N: <0.11		4, 10, 18–23, 32
Mrk 279	Sy 1	0.031	Y: 1.0	Y: 2.6		N: <0.07		8, 18, 20–22
Mrk 509	Sy 1	0.0355	Y: 1.1	Y: 3.5–4.5	N	N: <0.08		8, 19–23
ESO 141−G55	Sy 1	0.037	Y: 0.6	Y(3 σ): ~3	N	N: <0.15		8, 18–22
Cen A	RG, Sub, Sy 2	0.0008	Y: 28.	Y: 25.–63.	Y	N: <0.15	Y(?)	12, 15, 16, 18, 22, 23, 33–47, 88, 90
NGC 1275	RG, Sub, Sy 2	0.0183	Y: 3.3	N: <2.4		N: <0.09	N	8, 18, 20–24, 87
3C 120	Sy 1, RG, SL	0.0334	Y: 1.8	Y: 2.1–3.9	N	N: <0.09		8, 18–23
3C 111	Sy 1, RG, SL?	0.049		Y: 2.1–3.1	N	N: <0.09	N	18–22, 24, 48
3C 390.3	Sy 1, RG, SL?	0.0569	Y: 3.0	Y: <1.5–4.1		N: <0.07		8, 18, 20–22, 48
Mrk 421 (1101+384)	FS, BL	0.031	Y	N: <0.9		Y: 0.14	Y: 1.5	10, 18, 21, 23, 24, 49–53, 88
PKS 0521−365	FS, HP	0.055				Y(4 σ): ~0.2		23, 54, 88, 91
PKS 2005−489	FS, BL, OV	0.071				Y(4 σ): ~0.18		23, 88
1219+285	FS, BL, HP, OV	0.102				Y: 0.17		88
PKS 2155−304	BL	0.117		Y: <2.1–4.9		N		18, 21, 23, 51
3C 273 (1226+023)	FS, SL, HP, OV	0.158	Y	Y: 3.6–19.7	Y	Y: <0.13–0.21	N	12, 15, 16, 18, 21, 23, 24, 38, 45, 51, 53, 55–67, 88, 92
0829+046	FS, BL, OV	0.18				Y(4 σ): ~0.14		23, 88
PKS 1510−089	FS, HP, OV?	0.361				Y: 0.18–0.23		23, 68, 88
0954+658	FS, BL, HP	0.368				Y: 0.21		88
4C 21.35 (1222+216)	FS	0.435				Y: 0.17		88
3C 279 (1253−055)	FS, SL, HP, OV	0.538		Y: <2.4–6.2	Y	Y: 0.9–2.7	N	18, 21, 23, 24, 45, 51, 53, 64, 69, 70, 88
1E 1227+0224	QSO (near 3C 273)	0.57		Y(SIGMA)				15, 71, 72
4C 29.45 (1156+295)	FS, SL, HP, OV	0.729				Y: 0.63		53, 88
PKS 0454−463	FS	0.858				Y: <0.16–0.29		23, 53, 88
3C 454.3 (2251+158)	FS, SL, HP, OV	0.859		Y: <2.2–4.5	Y(?)	Y: 0.8–1.35	N	23, 24, 51, 53, 66, 73, 74, 88, 93
PKS 0537−441	FS, BL, HP	0.894				Y: 0.17–0.32		23, 53, 75, 88
PKS 0420−014	FS, HP, OV	0.92				Y: <0.14–0.45		23, 53, 76, 88
PKS 0235+164	FS, BL, SL?, HP	0.94				Y: <0.3–0.82		23, 53, 66, 77, 88
PKS 1933−400	FS	0.966				Y(4 σ): ~0.88		23, 88

TABLE 1—*Continued*

ACTIVE GALACTIC NUCLEI DETECTED AT >20 keV

Source	Type	z	20–165 keV	50–150 keV	1–30 MeV	>100 MeV	>0.5 TeV	Reference
PKS 0208−512	FS, HP	1.003				Y: 0.4–1.1		23, 53, 66, 78, 88
PKS 0454−234	FS, HP	1.009				Y(4 σ): ~0.14		23, 63, 88
CTA 102 (2230+114)	FS, SL?, HP	1.037		Y: <1.6–4.0	Y(?)	Y: 0.25–0.46		23, 51, 53, 74, 79, 88, 93
PKS 1229−021	FS	1.045				Y(4 σ): ~0.12		23, 88
PKS 1741−038	FS, HP	1.054				Y: 0.2–0.34		23, 88
PKS 2356+196	FS	1.066				Y(4 σ): ~0.29		23, 63, 88
PKS 0506−612	FS	1.093			Y(?)	Y(4 σ): ~0.06		23, 62, 88, 89
PKS 0446+112	FS	1.207				Y: <0.16–1.04		23, 66, 88
PKS 1313−333	FS	1.21				Y: 0.1–1.3		23, 88
4C 28.07 (0234+285)	FS, SL, HP	1.213				Y: 0.16		23, 53, 88
4C 10.45 (1606+106)	FS	1.23				Y: 0.27–0.53		23, 53, 88
4C 51.37 (1739+522)	FS	1.38				Y: 0.36		53, 88
1611+343	FS, OV	1.40				Y: 0.33		53, 88
0804+499	FS, HP	1.43				Y: 0.29		23, 63, 88
PKS 2052−474	FS	1.489				Y: 0.26		23, 53, 80, 88
PKS 1406−076	FS	1.494				Y: <0.10–0.41		23, 53, 66, 81, 88
4C 38.41 (1633+382)	FS, SL, OV	1.81				Y: 1.0	N	23, 24, 53, 64, 66, 82, 88
0827+243	FS, OV	2.046				Y: 0.21		23, 53, 88
PKS 0528+134	FS, OV	2.06		Y: 2.0–4.5	Y	Y: <0.5–1.6	N	18, 21, 23, 24, 45, 51, 53, 64, 66, 83, 84, 88
4C 71.07 (0836+710)	FS, SL, HP	2.17				Y: 0.14–0.34	N	23, 24, 53, 63, 64, 88
PKS 0458−020	FS, OV	2.286				Y(4 σ): ~0.28		23, 88
4C 15.05 (0202+149)	FS, HP	?		N: <8.7		Y: 0.26		23, 51, 53, 75, 88
0716+714	FS, BL, SL?, HP	?		N: <1.2		Y: 0.2–0.5	N	23, 24, 51, 53, 85, 88, 91
4C 15.54 (1604+159)	BL, HP	?				Y(4 σ): ~0.17		23, 88
PKS 1622−253	FS	?				Y: 0.19–0.47		23, 53, 86, 88
2022−077	FS	?				Y: <0.15–0.63		23, 53, 88
PKS 2209+236	FS	?				Y(4 σ): ~0.15		23, 88
H1517+656	BL	?		Y: 4.9				51

Type: Sy = Seyfert, RG = radio galaxy, Sub = subluminal, SL = superluminal, FS = flat spectrum radio galaxy, BL = BL Lac, HP = high optical polarization, OV = optically violent variable (OVV).

NOTE 1.—With some exceptions, the columns refer to detections by instruments as follows: 20–165 keV: *HEAO 1*, *Exosat*, and *Ginga*; 50–150 keV: OSSE and SIGMA; 1–30 MeV: COMPTEL; >100 MeV: EGRET; >0.5 TeV: Whipple.

NOTE 2.—A "Y" indicates a detection of significance greater than 5.0 σ for the >100 MeV column and greater than 3.5 σ for the other columns. The significance level for marginal detections is given in parentheses, where, for example, 3 σ means between 2.5 $\sigma \leq$ significance < 3.5 σ.

NOTE 3.—Numbers in detection columns are fluxes where available. Units and references are: 20–165 keV: 10^{-3} ph cm^{-2} s^{-1} (Rothschild et al. 1983, from luminosities in their Table 2; NGC 4151 from Baity et al. 1984; MCG +8−11−11 from Ubertini et al. 1984; Cen A from Baity et al. 1981); 50–150 keV: 10^{-4} ph cm^{-2} s^{-1} (Johnson et al. 1994; 0.1 MeV times numbers in their Table 1); >100 MeV: 10^{-6} ph cm^{-2} s^{-1} (Fichtel et al. 1994; Lin et al. 1993; von Montigny et al. 1994); >0.5 TeV: 10^{-11} ph cm^{-2} s^{-1} (Punch et al. 1992).

REFERENCES.—(1) Baity et al. 1975; (2) Paciesas et al. 1977; (3) Auriemma et al. 1978; (4) Frontera et al. 1979; (5) Beall et al. 1981; (6) Coe et al. 1981; (7) Perotti et al. 1981a; (8) Rothschild et al. 1983; (9) Baity et al. 1984; (10) Ubertini et al. 1984; (11) Bassani et al. 1986; (12) Maisack et al. 1992; (13) Perotti et al. 1991; (14) Jourdain et al. 1992b; (15) Bassani et al. 1992; (16) Paciesas et al. 1993a; (17) Maisack et al. 1993; (18) Cameron et al. 1993; (19) Maisack et al. 1994; (20) Lin et al. 1993; (21) Kurfess 1994; (22) Johnson et al. 1994; (23) Fichtel et al. 1994; (24) Schubnell et al. 1994; (25) Madejski et al. 1993; (26) Paul 1994; (27) Fabian et al. 1993; (28) Madejski et al. 1995; (29) Schachter & Elvis 1994; (30) Matt et al. 1990; (31) Rothschild et al. 1979; (32) Perotti et al. 1981b; (33) Grindlay et al. 1975; (34) Hall et al. 1976; (35) Mushotzky et al. 1976; (36) Mushotzky et al. 1978; (37) Baity et al. 1981; (38) Pietsch et al. 1981; (39) Gehrels et al. 1984; (40) von Ballmoos et al. 1987; (41) Bond et al. 1990; (42) Brazier et al. 1990; (43) Jourdain et al. 1993; (44) Paciesas et al. 1993b; (45) Collmar et al. 1993; (46) Ubertini et al. 1993; (47) Kinzer et al. 1994; (48) Mushotzky et al. 1977; (49) Lin et al. 1992; (50) Punch et al. 1992; (51) McNaron-Brown et al. 1994, 1995; (52) Lin et al. 1994; (53) Hartman et al. 1994; (54) Thompson et al. 1992; (55) Swanenburg et al. 1978; (56) Bignami et al. 1979; (57) Primini et al. 1979; (58) Bezler et al. 1984; (59) Damle et al. 1987; (60) Dean et al. 1990; (61) Bassani et al. 1991; (62) Hermsen et al. 1993; (63) von Montigny et al. 1993; (64) Fennell et al. 1993; (65) Lichti et al. 1994; (66) Michelson et al. 1994; (67) Paciesas et al. 1994; (68) Thompson et al. 1993b; (69) Hartman et al. 1992a; (70) Kniffen et al. 1993; (71) Jourdain et al. 1992b; (72) Grindlay 1993; (73) Hartman et al. 1993; (74) Blom et al. 1994; (75) Thompson et al. 1993a; (76) Hartman et al. 1992b; (77) Hunter et al. 1993b; (78) Bertsch et al. 1993; (79) Nolan et al. 1993; (80) Fichtel 1993; (81) Dingus et al. 1993; (82) Mattox et al. 1993; (83) Hunter et al. 1993a; (84) Collmar et al. 1994; (85) Michelson et al. 1992; (86) Hunter et al. 1994; (87) Osako et al. 1995; (88) von Montigny et al. 1994; (89) Bloemen et al. 1995; (90) Kinzer et al. 1995; (91) Lin et al. 1995; (92) Johnson et al. 1995; (93) Blom et al. 1995.

TABLE 2

BENCHMARK OPERATING CHARACTERISTICS OF GAMMA-RAY TELESCOPES

	Compton Gamma Ray Observatory					
	BATSE	COMPTEL	EGRET	OSSE	SIGMA/*Granat*	Whipple
Field of View[a]	4π[b]	$\sim 30°$	$\sim 20°$	$3.8° \times 11.4°$	$4.3° \times 4.7°$[c]	3°
Source Localization[a]	$\sim 3°$ (strong burst)	1.7°–4.4°	0.1°–0.5° (strong source)	$\sim 1°$ $\sim 0.1°$ (strong source)	$\sim 13'$	0.2°
Energy Range (MeV)	0.02–1.9 (LAD)[d] 0.01–100 (SD)[d]	0.8–30	$20–3 \times 10^4$	0.05–10	0.035–1.3	2×10^5–2×10^7[e]
Energy Resolution $\Delta E/E$	8% at 0.66 MeV (SD)[d]	5%–8%	$\sim 20\%$ at 100 MeV	$\sim 8\%$ at 600 keV	$\sim 12\%$ at 122 keV	$\sim 40\%$
Continuum Sensitivity (ergs cm^{-2} s^{-1})	$\sim 10^{-9}$ ($0.05 < E < 0.3$)[f]	$\sim 5 \times 10^{-11}$ ($1.0 < E < 10$)[g]	$\sim 10^{-11}$ ($E \sim 100$ MeV)[g]	$\sim 6 \times 10^{-11}$ ($0.1 < E < 1$)[g]	$\sim 4 \times 10^{-10}$ ($0.04 < E < 0.4$)	1.6×10^{-11}[e]

[a] FWHM values given where applicable.
[b] Minus solid angle from Earth occultation.
[c] Field-of-view fully coded by aperture mask.
[d] LAD: Large Area Detector; SD: Spectroscopy Detector.
[e] Assuming $E^{-2.5}$ spectrum for an observing time of $\sim 1.5 \times 10^4$ s.
[f] Occultation sensitivity for one day.
[g] Nominal observing time of $\sim 5 \times 10^5$ s.

1993), and Cen A is only weakly detected with COMPTEL in the 0.75–1.0 MeV band by combining data from three observing periods (Collmar et al. 1993). The quasars 3C 273 and 3C 279 have been detected with both the OSSE (Johnson et al. 1995; McNaron-Brown et al. 1994, 1995) and COMPTEL (Schönfelder 1994; Williams et al. 1995) instruments. Forty-four AGNs have now been reported as sources of $E > 100$ MeV gamma rays (Fichtel et al. 1994; Hartman et al. 1994; von Montigny et al. 1995). The identification of these sources with AGNs that display blazar properties, which include high optical polarization, rapid optical variability, flat-spectrum radio emission from a compact core, and apparent superluminal motion, suggests that the $E > 100$ MeV gamma rays are produced in association with a radio jet (e.g., Dermer & Schlickeiser 1992).

The EGRET source Mrk 421, a BL Lac object, has also been viewed with OSSE but not positively detected. PKS 0538+134, a flat spectrum radio quasar, was observed in early viewing periods with only limited exposure (a total of 1.1×10^5 s with only two detectors; McNaron-Brown et al. 1994, 1995), and only a weak detection with OSSE is claimed. A solid (>5 σ) detection is reported, however, during VP 322 (McNaron-Brown et al. 1995). PKS 0528+134 has, moreover, been detected with COMPTEL (Collmar et al. 1994). Although the EGRET and OSSE observations were not contemporaneous, the combined OSSE, COMPTEL, and EGRET spectra of PKS 0528+134 implies that the spectrum of this source softens between the hard X-ray and medium-energy gamma-ray regimes. Indeed, contemporaneous observations by EGRET (Hartman et al. 1992a; von Montigny et al. 1993) and COMPTEL (Hermsen et al. 1993; Lichti et al. 1994; Johnson et al. 1995; see also McNaron-Brown et al. 1994, 1995) directly show spectral softening between ~ 1 and 30 MeV in both 3C 273 and 3C 279, indicating that spectral softening may be a general characteristic of gamma-ray emission from blazars.

3. CLASSIFICATION OF AGNS DETECTED AT GAMMA-RAY ENERGIES

It is important to establish whether the probability of detection of an active galaxy is related to the energy range in which it is observed, and whether this probability is correlated with source type. For this purpose, we calculate the hardness ratios between hard and soft gamma-ray energy bands. Figure 1*a* shows the ratios of the integrated $E > 100$ MeV photon flux (Fichtel et al. 1994; Montigny et al. 1995) or upper limits (Lin et al. 1993) measured with EGRET to the integrated 50–150 keV flux measured with OSSE (Johnson et al. 1994; McNaron-Brown et al. 1995) as a function of radio spectral luminosity at 1.4 GHz, assuming isotropic radio emission. For the gamma-ray hardness ratios, we use the maximum OSSE flux measured for sources with positive detections in the 50–150 keV range. The vertical extent of the hardness ratios for positive EGRET detections reflects the range of flux values arising from source variability, not measurement error. Note that most observations are not contemporaneous. In order to make a uniform comparison, the calculation of the radio spectral luminosity at 1.4 GHz uses the total measured radio flux densities, including both compact and extended emission. The radio data for the Seyferts are from Giuricin et al. (1990), and the data for the radio galaxies and quasars are from Wall & Peacock's (1985) catalog.

Figure 1*a* shows that the Seyferts and radio galaxies do not radiate $E > 100$ MeV gamma rays in the same proportion, compared to their soft γ-ray emissions, as do the blazars. For the most extreme cases, namely NGC 4151, Cen A, and 3C 279, the hardness ratios differ by approximately two orders of magnitude. Moreover, those sources with the brightest inferred radio luminosity also show the greatest $E > 100$ MeV gamma-ray emission. In Figure 1*b* we plot the $E > 100$ MeV luminosity versus the 50–150 keV luminosity for these sources, assuming isotropic emission in the luminosity calculations. We see that the luminosities of the soft gamma-ray spectrum Seyferts and radio galaxies cluster in the range 10^{41}–10^{44} ergs s^{-1}, whereas the quasars are more luminous by roughly three orders of magnitude in the OSSE energy range. The major exception is Mrk 421, a BL Lac object which has a luminosity $\lesssim 2 \times 10^{43}$ ergs s^{-1} in the OSSE energy range.

The clearcut distinction between the distance scales for Seyferts and radio galaxies on the one hand and blazars on the other is shown in Figure 2, where the redshift distributions of the different types of objects are plotted. From this figure we see that the gamma-ray soft Seyferts and radio galaxies (Fig. 2*a*) have a qualitatively different distance distribution than the

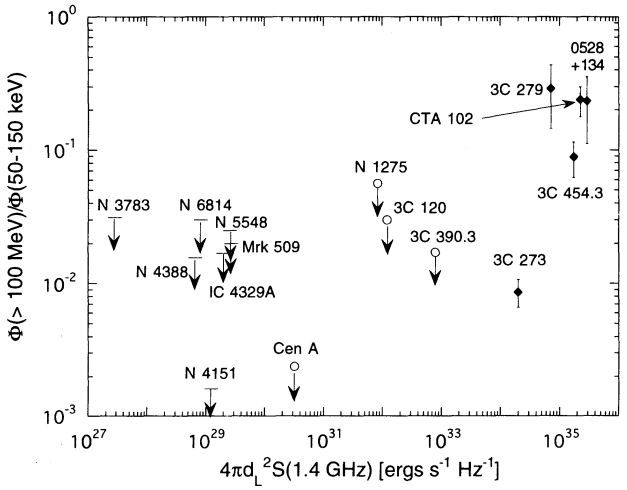

FIG. 1a

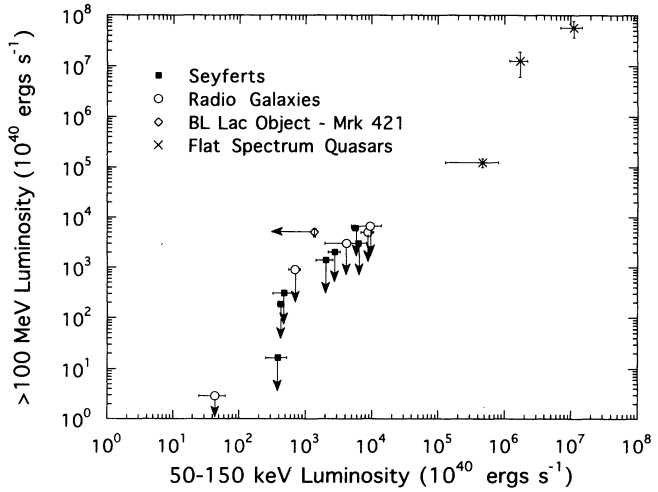

FIG. 1b

FIG. 1.—Hardness ratios and luminosities of gamma-ray AGNs. In Fig. 1*a* we show the ratio of integrated $E > 100$ MeV photon flux measured with EGRET to the integrated photon flux between 50 keV and 150 keV measured with OSSE. This is plotted as a function $4\pi d_L^2 S(1.4\ \mathrm{GHz})$, which is a measure of the radio spectral luminosity at 1.4 GHz, assuming isotropic emission. Here d_L is the luminosity distance and $S(1.4\ \mathrm{GHz})$ is the 1.4 GHz radio flux density. Seyfert galaxies are denoted by horizontal lines, radio galaxies by circles, and quasars by filled diamonds. In Fig. 1*b*, we plot the inferred isotropic luminosity in the $E > 100$ MeV band vs. the luminosity in the 50–150 keV band for Mrk 421 and 3C 111 in addition to the sources shown in Fig. 1*a*.

gamma-ray hard blazars (Fig. 2*b*). The detected Seyferts and radio galaxies are nearby ($z \lesssim 0.06$) whereas the blazars are seen out to redshift $z \gtrsim 2$. This is not a function of relative instrument sensitivities, as shown in Figure 1*a*. Again, we find compelling evidence for (at least) two classes of gamma-ray AGN.

We also plot in Figure 2*b* the redshift distribution of 350 flat-spectrum radio quasars (FSRQs) from the Parkes radio catalog (PKSCAT90, version 1.01, updated from Bolton et al. 1979). Compared with the redshift distribution of the radio sources, there is some suggestion of structure in the blazar redshift distribution, namely a clumping at $z \sim 1.0$ and 2.0. The detection of gamma rays from BL Lacs at redshifts smaller than the average redshift of the entire gamma-ray blazar sample is also indicated. However, the small blazar sample size does not allow a strong conclusion to be reached. A Kolmogorov-Smirnov two-sided test shows that the hypothesis that the 38 EGRET gamma-ray blazars with known redshift are drawn from the same population as the FSRQs can only be rejected at the ~80% level. In the absence of better statistics, we are not justified in arguing that the gamma-ray blazar and FSRQ redshift distributions are statistically different. Alternately, we can conclude that there is no strong evidence against the association of gamma-ray blazars and

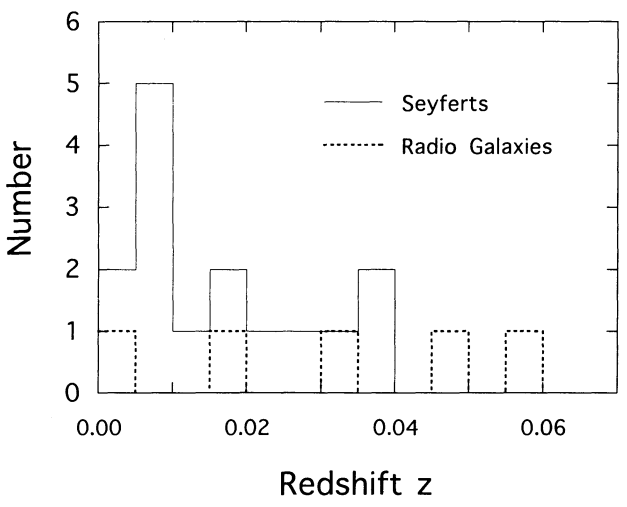

FIG. 2a

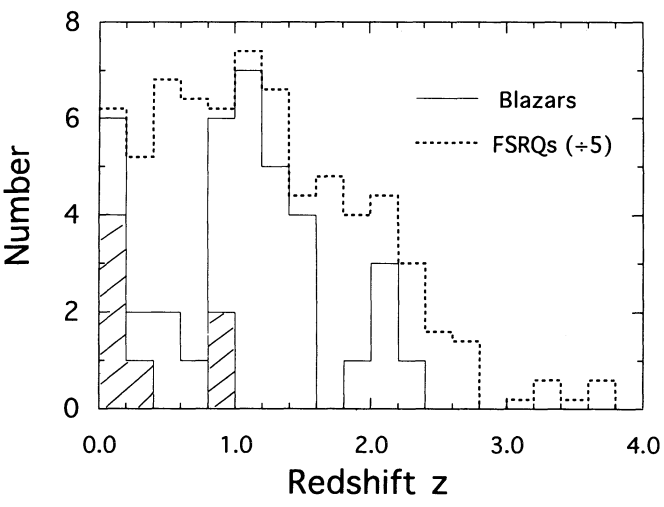

FIG. 2b

FIG. 2.—Redshift distributions of AGNs detected at photon energies $E > 50$ keV (see Table 1). (*a*) Redshift distribution of Seyferts and radio galaxies. (*b*) Redshift distribution of blazars, with subset of BL Lac objects shown by the cross-hatched histogram. Also shown for comparison by the dotted histogram is the redshift distribution of flat-spectrum radio sources from the Parkes radio catalog with measured redshift. Note the change of scale for redshift z in Figs. 2*a* and 2*b*.

FSRQs. We consider the implication of the redshift distributions in more detail in § 5.

We find therefore that the luminosities, redshift distributions, and gross spectral features of the high-energy emission of radio galaxies and Seyfert 1's are similar and are distinct from blazars. This suggests that the X-rays and gamma rays from Seyferts and radio galaxies are produced by a different mechanism than the mechanism which makes the blazar radiation. An obvious possibility is that the $E > 100$ MeV blazar gamma-ray emission is associated with emission from a jet viewed at small angles with respect to the jet axis. Superluminal motion can occur in this situation and is the best indication of jets observed with an axis directed at small angles with respect to the viewing direction. Thus if the Seyfert and blazar radiation mechanisms are distinct, we could expect that the gamma-ray spectral properties of radio-loud AGNs should be correlated with the appearance of superluminal motions: no superluminal or subluminal motion should correspond to a Seyfert nucleus with virtually no $E > 100$ MeV gamma-ray jet emission, whereas sources with increasingly large superluminal velocities should be accompanied by the $E > 100$ MeV jet emissions. In Table 3, we list values of apparent transverse velocities measured for the gamma-ray AGNs listed in Table 2, using the compilations of Porcas (1987), Impey (1987), Vermeulen & Cohen (1994), and the recent report of Pohl et al. (1995) for PKS 0528+134. We also include in Table 3 radio-quiet gamma-ray AGNs for which detection of superluminal motion through VLBI techniques is difficult or impossible. With the improved imaging of the *Hubble Space Telescope*, however, the detection of superluminal motion at optical wavelengths is feasible, and such detections would severely impact current models of radio-quiet Seyferts.

The radio galaxies Cen A and NGC 1275 have so far displayed only subluminal motions, and have not been reported as strong sources in the EGRET energy range. Approximately one-quarter of the EGRET blazars do exhibit apparent superluminal motion. But two (3C 120, 3C 111) and perhaps three (3C 390.3) of the five gamma-ray emitting radio galaxies which do not radiate in the EGRET range also show strong evidence for apparent superluminal motion. Thus it does not follow that the appearance of superluminal motion is correlated with the appearance of $E > 100$ MeV emission. But it is interesting to note that the average superluminal velocity for the gamma-ray blazars with measured superluminal motions is systematically greater than that for the radio galaxies. It is therefore possible that the $E > 100$ MeV gamma-ray emissivity falls off strongly beyond the superluminal angle $\theta_{SL} = \cos^{-1}(\beta_\Gamma)$, where $\beta_\Gamma c$ is the velocity of the outflowing plasma that produces the jet. Superluminal motion could still be detected at these relatively large angles. We might therefore expect that radio galaxies will show intermediate gamma-ray properties between Seyferts and blazars. The relatively harder gamma-ray spectrum of Cen A compared to the typical Seyfert spectra has been noted, but attributed to Compton-scattered jet radiation (Skibo, Dermer, & Kinzer 1994). An interesting test is provided by the gamma-ray emitting radio galaxies which show evidence for superluminal motion. Because 3C 120 has the firmest evidence for superluminal motion (Walker, Benson, & Unwin 1987), whereas the evidence is weaker for 3C 111 (Impey 1987) and much weaker for 3C 390.3 (Porcas 1987), we expect that 3C 120 is the most likely of the three sources to have significant $E > 100$ MeV jet emission and be observable with EGRET, although no positive EGRET detection has yet been reported for any of these sources.

4. SPECTRA

4.1. *Two Classes of Spectra*

We now directly compare spectral shapes of AGNs in the gamma-ray region. For this comparison, good statistics are required so that only the brightest AGNs can be used. Figure 3 shows the $E > 0.1$ keV EL_E power spectra for the brightest radio-quiet Seyferts, NGC 4151 and IC 4329A, the BL Lac object Mrk 421, and the quasar 3C 279. The differential power spectra were normalized by multiplying the measured fluxes by $4\pi d_L^2$, where d_L is the luminosity distance. Throughout this paper we adopt a $q_0 = \frac{1}{2}$ cosmology with a Hubble constant $H_0 = 75h$ km s^{-1} Mpc^{-1} with $h = 1$. Quasi-contemporaneous data for NGC 4151 are from *Ginga* (Yaqoob et al. 1993; epoch 1991 May 31–June 2) and OSSE (Maisack et al. 1993; epoch 1991 June 28–July 12) observations. The data for IC 4329A were obtained in a simultaneous *ROSAT* and OSSE observation in 1993 January by Fabian et al. (1993) and Madejski et al. (1995), to which they added nonsimultaneous *Ginga* data from Fiore et al. (1992) and Piro, Yamauchi, & Matsuoka (1990). The data for Mrk 421 are from nonsimultaneous EGRET (Lin et al. 1992), *Ginga* (Makino et al. 1987), and Whipple (Mohanty et al. 1993) observations. The data for 3C 279 are from COMPTEL (Collmar et al. 1993) and EGRET (Hartman et al. 1992a) observations during its flaring episode in 1991 June. The X-ray data for 3C 279 are from contemporaneous *Ginga* (Makino et al. 1993) observations. We also show the upper limit for 3C 279 obtained with the Whipple Observatory (Fennell et al. 1993).

As can be readily seen, there is a clear distinction between the spectra of the Seyferts and the blazars. The Seyfert spectra cut off above $\sim$50–100 keV, whereas the spectra of Mrk 421 and 3C 279 are extremely hard, with $s \approx 1.5$ below $\sim$10 MeV, and then steepening to $s \approx 2$ at energies from 100 MeV to $\gtrsim$10 GeV. The NGC 4151 gamma-ray spectrum can be well fitted with a Sunyaev-Titarchuk (1980) thermal Comptonization spectrum with temperature $kT \cong 40$ keV and optical depth $\tau \cong 3$ (Maisack et al. 1993; Titarchuk & Mastichiadis 1994). Its spectral shape indicates that the emission is primarily thermal, although some small nonthermal component could also be present (Zdziarski, Lightman, & Maciolek-Niedźwiecki 1993). The blazar spectra, on the other hand, are distinctly nonthermal, with the bulk of the high-energy emission radiated in the medium-energy gamma-ray regime. We now consider the spectral differences of the two classes in detail.

4.2. *Seyfert Galaxies*

NGC 4151 is the nearest Seyfert ($z = 0.0033$) and the brightest radio-quiet AGN at soft gamma-ray energies. The softening of its spectrum above $\sim$50 keV was first clearly detected in 1990 with the SIGMA telescope on *Granat* (Jourdain et al. 1992a). There was also weak evidence for softening in one of three *HEAO 1* observations in 1978 June (Baity et al. 1984). The OSSE observations (Maisack et al. 1993) now clearly show the exponential nature of the cutoff, indicating that the hard X-rays and soft gamma rays have a primarily thermal origin (e.g., Zdziarski et al. 1993; Titarchuk & Mastichiadis 1994).

Although NGC 4151 is the best-studied Seyfert AGN, it is probably not the best prototype for a Seyfert 1 spectrum since it sometimes shows Seyfert 2 properties and is technically classified as a Seyfert 1.5 (Ayani & Maehara 1991). A better example may be IC 4329A, a standard Seyfert 1 at $z = 0.016$. The evidence for a cutoff in the IC 4329A spectrum at high

TABLE 3

APPARENT SUPERLUMINAL MOTION OBSERVATIONS OF GAMMA-RAY AGNs

Source	Other Name	z	Source Type[a]	$h\beta_{app} \pm h\Delta\beta_{app}$[a]
0202+149		?	[b]	
0208−512		1.003	[b]	
0234+285		1.213	[b]	6.97 ± 3.49
0235+164		0.94	[b] (I)	~22
0316+413	NGC 1275, 3C 84	0.0183	[c]	0.32 ± 0.08
0415+379	3C 111	0.049	[c]	2.56 ± 0.33
0420−014		0.92	[b]	
0430+052	3C 120	0.0334	[c]	1.55, 2.89, 3.79, 3.05, 2.91
0446+112		1.207	[b]	
0454−463		0.858	[b]	
0454−234		1.009	[d]	
0458−020		2.286	[d]	0.0
0506−612[e]		1.093	[d]	
0521−365		0.055	[d]	
0528+134		2.06	[b] (Pohl)	4.0 ± 1.0
0537−441		0.894	[b]	
0551+464	MCG +8−11−11	0.0205	[f]	
0716+714[g]		?	[b]	
0804+499		1.43	[d]	
0827+243		2.046	[b]	
0829+046		0.18	[d]	
0836+710		2.17	[b]	7.17 ± 1.56, 0.0, 4.37 ± 1.56
0945−307	MCG −5−23−16	0.0082	[f]	
0954+658		0.368	[h]	
1101+384	Mrk 421	0.031	[b]	1.43 ± 0.02, 1.01 ± 0.17
1136−375	NGC 3783	0.0092	[f]	
1156+295		0.729	[d]	19.58
1208+397	NGC 4151	0.0033	[f]	
1219+285		0.102	[h]	
1222+216		0.437	[h]	
1223+129	NGC 4388	0.0087	[f]	
1226+023	3C 273	0.158	[b]	5.78 ± 0.76, 4.0 ± 0.2, 4.98 ± 1.21, 6.03 ± 0.15, 3.27 ± 0.45, 3.82 ± 0.26, 4.63 ± 0.56, 4.1 ± 0.6
1227+024		0.57	[i]	
1229−021		1.045	[d]	
1253−055	3C 279	0.538	[b]	6.89 ± 1.38, 1.65 ± 0.28
1313−333		1.21	[d]	
1322−428	Cen A	0.0008	[c]	0.11 ± 0.02
1333−340	MCG −6−30−15	0.0078	[f]	
1346−300	IC 4329A	0.0157	[f]	
1351+695	Mrk 279	0.031	[f]	
1406−076		1.494	[b]	
1415+254	NGC 5548	0.017	[f]	
1510−089		0.361	[b]	
1517+656		?	[j]	
1604+159		?	[d]	
1606+106		1.23	[b]	
1611+343		1.40	[h]	
1622−253		?	[b]	
1633+382		1.81	[b]	
1739+522		1.38	[h]	
1741−038		1.054	[b]	
1845+797	3C 390.3	0.0569	[c] (P)	1.4
1916−587	ESO 141−G55	0.037	[f]	
1933−400		0.966	[d]	
1939−104	NGC 6814	0.0053	[f]	
2005−489		0.071	[d]	
2022−077		?	[b]	
2041−109	Mrk 509	0.0355	[f]	
2052−474		1.489	[b]	
2155−304		0.117	[j]	
2209+236		?	[d]	
2230+114	CTA 102	1.037	[b] (P, I)	0.0 ± 10.6, 13.5
2251+158	3C 454.3	0.859	[b]	0.86 ± 0.30, −0.87 ± 1.36, 6.63 ± 1.14, 3.98 ± 0.95
2315−426	NGC 7582	0.0049	[f]	
2356+196		1.066	[d]	

[a] Apparent superluminal velocities from Vermeulen & Cohen (1994), except where indicated (P): Porcas (1987); (I): Impey (1987); (Pohl): Pohl et al. (1995). $H_0 = 75h$ km s^{-1} Mpc^{-1}.

[b] EGRET source—strong detection: Phase 1 catalog.

[c] Radio galaxies detected with OSSE.

[d] EGRET source—marginal detection: Phase 1 catalog.

[e] COMPTEL blazar (Bloemen 1995).

[f] Radio-quiet Seyfert galaxies detected with OSSE.

[g] Superluminal source if $z \gtrsim 0.3$.

[h] EGRET sources reported after Phase 1.

[i] SIGMA QSO—1227+024.

[j] OSSE blazars—PKS 2155−304 and H 1517+656 (neither were detected with EGRET and both are BL Lac objects).

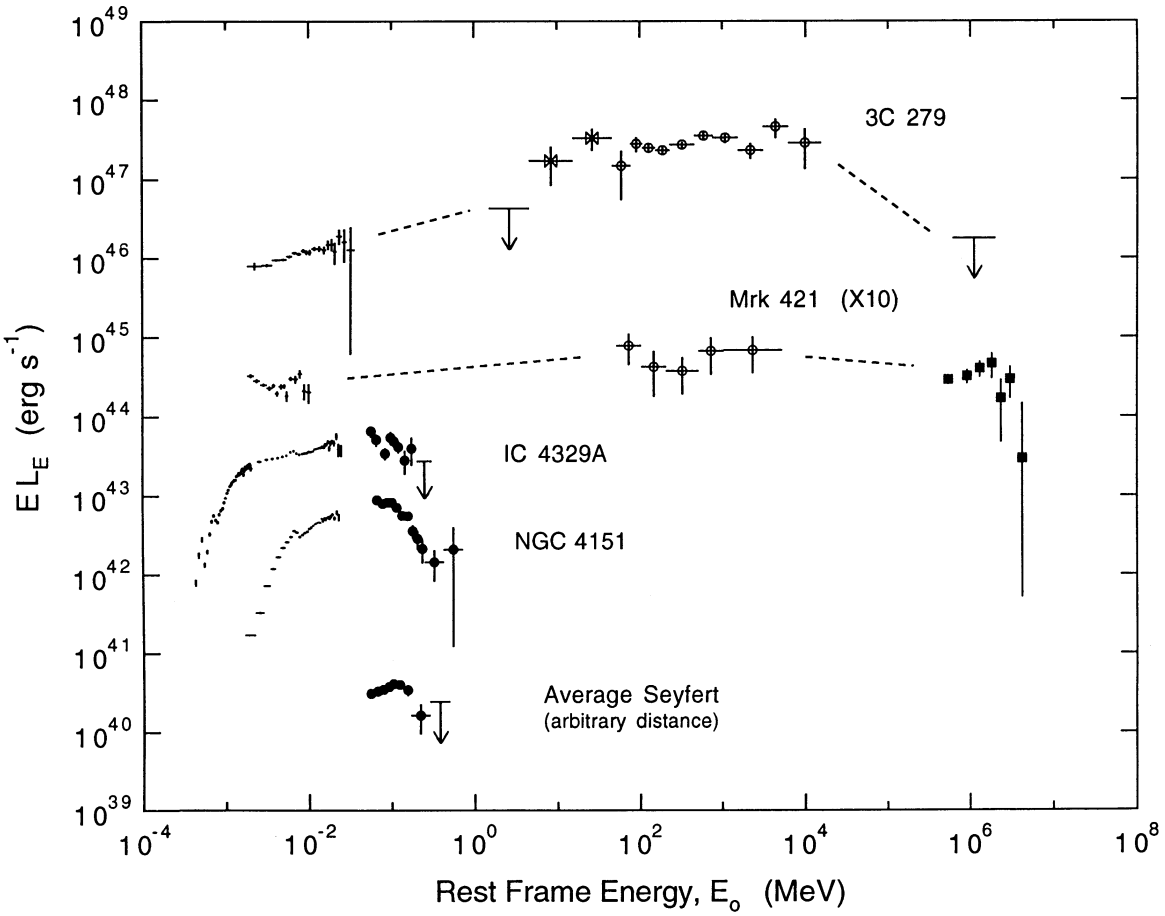

FIG. 3.—Power spectra for NGC 4151, IC 4329 A, Mrk 421, and 3C 279, assuming isotropic emission. Here we plot the luminosity per natural logarithmic energy interval, $EL_E = 4\pi d_L^2 E^2 \Phi(E)$, as a function of rest-frame energy $E_0 = (1 + z)E$, where $\Phi(E)$ is the flux (photons cm^{-2} s^{-1} MeV^{-1}) and d_L is the luminosity distance. A Hubble constant $H_0 = 75$ km s^{-1} Mpc^{-1} and deceleration parameter of $q_0 = \frac{1}{2}$ were assumed. Also shown is the average Seyfert spectrum. References for the data are given in the text. Note that the Mrk 421 spectrum is multiplied by 10.

energies is not as strong as for NGC 4151. X-ray observations of Seyfert AGNs show that Fe Kα emission features, absorption edges, and spectral hardenings at $E \gtrsim 10$ keV are most simply interpreted in terms of reflection of a large fraction of the high-energy radiation by cold, optically thick material, and transmission of the source radiation through warm absorbing gas with hydrogen column densities $\sim 10^{22}$–10^{23} cm^{-2} (e.g., Zdziarski et al. 1990; Nandra & Pounds 1994). This weakens the case that OSSE observations show significant spectral softening of Seyfert galaxies above ≈ 50–100 keV, since a softer input photon spectrum with $s \approx 2$, when added to a reflection component, reproduces the harder spectra observed with *HEAO 1* and *Ginga* between 2 and 10 keV. The best-fit model of Madejski et al. (1995) for IC 4329A does have an exponential cutoff with $kT \approx 300$ keV, but a flat spectrum in vF_v (i.e., $s = 2$) is also an acceptable fit.

We also show in Figure 3 the mean Seyfert spectrum in the soft gamma-ray regime, which was derived by Johnson et al. (1994) using OSSE data. This spectrum is the average of all Seyfert and radio-galaxy spectra with positive detections in the 50–150 keV column of Table 1, plus a few weak detections, but excluding the brightest objects NGC 4151, IC 4329A, NGC 4388, and Cen A, as well as NGC 4507 and ESO 141-G55. Being the average of Seyferts with relatively weak gamma-ray emission, the spectral flux is a factor of 5–10 below that of NGC 4151. Nevertheless, the mean Seyfert spectrum shows evidence for spectral softening at energies greater than ~ 100 keV. In fact, a power-law fit can be rejected at the 94% confidence level, but a good fit is obtained for a thermal Compton scattering model with temperature $kT = 30$ keV and optical depth $\tau_T \approx 5$ (Johnson et al. 1994).

4.3. *Blazars*

Of the 44 blazars detected by EGRET (>100 MeV column of Table 1), 17 have adequate detection significance for a good determination of the spectrum (Fichtel et al. 1994). In most cases the spectra can be well fitted with power laws, although the limited statistics usually permit some curvature. The average spectral index is $\langle s \rangle \cong 2.1$ with a spread of $\Delta s \cong \pm 0.35$. This narrow spread suggests that the production mechanism for the blazar gamma-ray emission produces a rather uniform power-law spectrum. There is, however, clear evidence for spectral breaks in the MeV range, with the typical spectral index $\lesssim 1.8$ below a few MeV (Schönfelder 1994; McNaron-Brown et al. 1994, 1995).

Above 10 GeV, the lack of detection of 3C 279 by ground-based Cerenkov telescopes (Fennell et al. 1993) implies that the observed spectrum must soften to $s > 2$ by the TeV range (see

Fig. 3). Only for the nearby BL Lac object Mrk 421 is there a ground-based detection (Punch et al. 1992), implying that the spectrum continues without break to at least TeV energies. Two possibilities for the lack of TeV detection of 3C 279 are that the source has intrinsic absorption of high-energy gamma rays by a soft photon radiation field near the central black hole that is not present in BL Lac objects (Dermer & Schlickeiser 1994), or that $\gamma-\gamma$ photon interactions between TeV gamma rays and intergalactic infrared radiation attenuate the flux for 3C 279 at $z = 0.54$, but not for Mrk 421 at $z = 0.03$ (Stecker, de Jager, & Salamon 1992). If intergalactic absorption is the correct explanation, then gamma-ray blazars generally emit a hard spectrum into the TeV regime. This model can be tested since it predicts that the Mrk 421 spectral break above several TeV, if due to intergalactic absorption (De Jager, Stecker, & Salamon 1994; see Fig. 3), must persist through all spectral changes in the source. This is not the case for intrinsic absorption, since the level of background radiation can change due to variations in the central source radiation. The recent outburst of Mrk 421 at TeV energies (Kerrick et al. 1994) could test this model.

4.4. *Multiwavelength Spectra and Transitional Objects: Cen A and* 3C 273

Multiwavelength spectra for NGC 4151, Cen A, 3C 273 and 3C 279 are shown in Figure 4 (see also Odenwald, Gehrels, & Howard 1994 and Gehrels & Cheung 1992 for other compilations). The various data sets are in general not contemporaneous. In the gamma-ray band, only *Compton* spectra are shown since they are generally of much better quality than previous observations. The spread in the data indicates the known range of variability.

The general characteristics of the multiwavelength spectrum of NGC 4151 is typical of gamma-ray bright Seyferts, and the spectrum of 3C 279 is typical of gamma-ray bright blazars such as PKS 0528+134 (Hunter et al. 1993a) and 3C 454.3 (Hartman et al. 1993). The spectrum of each object cuts off between 912 Å and the soft X-ray band due to the photoionization absorption by neutral hydrogen for photons with energies above the Lyman edge. The Seyfert spectra generally show more structure than the blazars, including an IR excess, UV/soft X-ray excesses, and a gamma-ray cutoff, whereas the blazar spectra have less structure, rise toward a dominant gamma-ray component, and are more variable in the radio-through-optical wavelengths than the Seyferts. The radio-optical emission of blazars is, however, less variable than the gamma-ray emission. Note the low level of radio flux for NGC 4151 as compared with the radio-loud objects. The IR excess for NGC 4151 is generally thought to be due to emission reprocessed by dust in the vicinity of the nucleus, whereas the variable flux for the radio-loud source suggests emission from the central source which is probably beamed. The soft X-ray attenuation of NGC 4151 is variable, implying a column depth

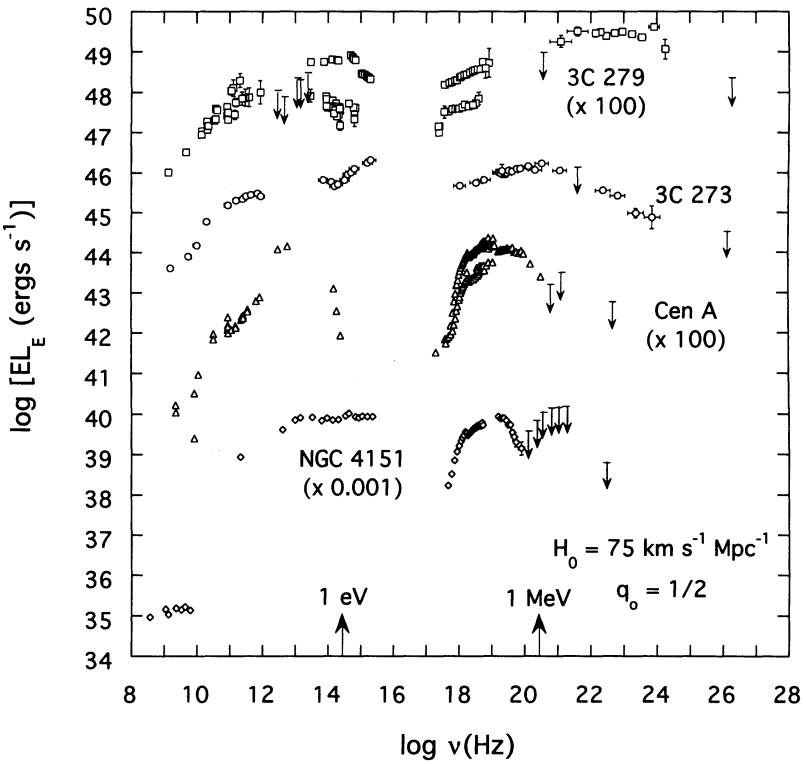

FIG. 4.—Multiwavelength power spectra for NGC 4151 (*triangles*), Cen A (*diamonds*), 3C 273 (*circles*), and 3C 279 (*squares*). The observations are generally not simultaneous in different frequency bands. The references for the radio-through-optical data of NGC 4151 are given in the compilation of Ramaty & Lingenfelter (1982). For Cen A, the radio data is from Meier et al. (1989), the submillimeter data is from Hawarden et al. (1993), the infrared data is given by Bailey et al. (1986), the X-ray data is from Morini, Anselmo, & Molteni (1989), and the soft gamma-ray data is from OSSE observations (Kinzer et al. 1994). The Cen A spectrum is a good representation of the nuclear radiation spectrum in view of the variability of the emission and the small beam sizes of the lower energy detectors. We also include the EGRET upper limit for Cen A (R. C. Hartman 1993, private communication). We use contemporaneous broadband data of Lichti et al. (1994) to construct the multiwavelenth spectrum of 3C 273, and the data of Makino et al. (1989) for 3C 279. Note that the *Ginga* data for 3C 279 given by Makino et al. (1993), which are contemporaneous with the EGRET observations and lie between the low and high state X-ray spectra shown, are not plotted here.

of 10^{22}–10^{23} H atoms cm^{-2} (Yaqoob et al. 1993). Its spectrum peaks at ~ 70 keV and then falls exponentially, consistent with a color temperature of ≈ 40 keV.

Two of the brighter and better studied AGNs, Cen A and 3C 273, are unusual objects and are not simply classified as gamma-ray Seyferts or blazars. Cen A is one of the nearest (3–5 Mpc) AGNs and the brightest radio-loud AGN at soft gamma-ray energies. It is a dusty elliptical with a bright active nucleus, and has inner jets and an extended radio source (see, e.g., Ebneter & Balick 1983). The soft X-ray attenuation gives a column depth of $\sim 10^{23}$ cm^{-2}. The spectrum for Cen A observed with OSSE (Kinzer et al. 1994) in 1991 is shown in Figure 4. Below ≈ 1 MeV it has a hard spectrum with $s \approx 1.8$ and then breaks to a softer power-law component with $s \approx 2.2$. This softening is observed in COMPTEL observations (Collmar et al. 1993). Cen A is not detected in the 100 MeV range (Fichtel et al. 1994), but has been detected one time at PeV energies with 4 σ significance (Grindlay et al. 1975). Later measurements (Hyland, Fenton, & Humble 1990; Brazier et al. 1990) did nor confirm the detection, but were not sensitive enough to disagree strongly.

The spectrum of 3C 273, the nearest quasar at $z = 0.158$, is considerably different than that of the typical gamma-ray blazar (see, e.g., Schönfelder 1994; Lichti et al. 1995; Johnson et al. 1995). As can be seen in Figure 4, the νF_ν spectrum peaks at a few MeV and then falls with $s \approx 2.5$ at energies much greater than 1 MeV. There is another peak in the optical/UV range which has been interpreted as the thermal emission from an accretion disk. In contrast to many gamma-ray blazars, the gamma-ray luminosity from 3C 273 does not dominate the power output.

5. INTERPRETATION OF THE TWO CLASSES OF GAMMA-RAY AGNS

We find that the inferred isotropic gamma-ray luminosities are in the range $\sim 10^{41}$–10^{44} ergs s^{-1} for Seyfert AGNs and radio galaxies and in the range $\sim 10^{45}$–10^{49} ergs s^{-1} for most BL Lacs and quasars (see Fig. 1*b*; Fichtel et al. 1994; Montigny et al. 1995). The redshifts of gamma-ray Seyfert AGNs and radio galaxies are clustered within $z \lesssim 0.06$, whereas the redshifts of gamma-ray blazars extend to $z \gtrsim 2$, with no statistically significant clustering at low redshifts (Fig. 2). The spectra of gamma-ray Seyferts and radio galaxies are very soft by comparison with the high-energy spectra of gama-ray blazars. Indeed, no Seyferts or radio galaxies have been detected at $E > 100$ MeV energies.

An interpretation apparently in accord with these results is that we are seeing comparatively weak, quasi-isotropic emission from the gamma-ray Seyferts, and beamed emission from collimated relativistic outflow from the gamma-ray blazars. Whether the gamma-ray emission from the radio galaxies is predominantly a Seyfert-type nucleus, scattered jet radiation (Skibo et al. 1994), or off-axis jet radiation is an open question. The existence of relativistic outflows from radio quasars was proposed by Blandford & Rees (1978) and Blandford & Königl (1979) in order to avoid the Compton catastrophe, and this model is also supported by observations of superluminal motion in blazars. Yet we see from Table 1 that although superluminal motion has been observed in $\gtrsim 20\%$ of the gamma-ray blazars, two (and possibly three) of the five radio galaxies detected at gamma-ray energies also show apparent superluminal motion. Thus it is not clear that the difference between the two classes represents emission from quasi-isotropic radiation on the one hand, and Doppler-boosted jet radiation on the other. In this section we consider whether the beaming model for blazars detected at gamma-ray energies is required by the gamma-ray evidence.

5.1. *Statistics of* AGNs *Detected at Gamma-Ray Energies*

We first ask whether the qualitatively different redshift distributions (Fig. 2) are due to beaming properties of relativistically outflowing matter. We denote the optically thin emissivity in the comoving fluid frame by $j'(\epsilon', \Omega')$ (ergs s^{-1} ϵ^{-1} sr^{-1} cm^{-3}), where $\epsilon = h\nu/m_e c^2$ is the dimensionless photon energy, $d\Omega$ is the element of solid angle in the direction $\Omega = (\mu, \phi)$, and primes denote quantities in the comoving frame. If V'_b is the volume of the comoving fluid element ("blob"), then the flux density $S(\epsilon; \Omega)$ (ergs s^{-1} ϵ^{-1} cm^{-2}) is just

$$S(\epsilon; \Omega) = d_L^{-2}\mathscr{D}^3(1+z)V'_b \times j'\left[\epsilon' = \frac{\epsilon(1+z)}{\mathscr{D}}, \mu' = \frac{\mu - \beta_\Gamma}{1 - \beta_\Gamma \mu}, \phi = \phi\right], \quad (1)$$

where Γ is the bulk Lorentz factor of the blob, $\beta_\Gamma c$ is its velocity, the Doppler factor $\mathscr{D} = [\Gamma(1 - \beta_\Gamma \mu)]^{-1}$, and d_L is the luminosity distance. For a $q_0 = \frac{1}{2}$ universe, $d_L = 2c[z + 1 - (z+1)^{1/2}]/H_0$.

We assume for simplicity that all blobs emit isotropically in the comoving fluid frame, so that $V'_b j'(\epsilon', \Omega') = (4\pi)^{-1} dL'(\epsilon')/d\epsilon'$. Assuming that the emission is a power-law in energy with energy spectral index α, we have $dL'(\epsilon')/d\epsilon' \propto \epsilon'^{-\alpha}$ for $\epsilon_l \le \epsilon' \le \epsilon_u$. Thus $V'_b j'(\epsilon', \Omega') = k_\alpha L \epsilon'^{-\alpha}/4\pi$ for $\epsilon_l \le \epsilon' \le \epsilon_u$, where $k_\alpha = (1-\alpha)(\epsilon_u^{1-\alpha} - \epsilon_l^{1-\alpha})^{-1}$ if $\alpha \ne 1$, and $k_\alpha = \ln^{-1}(\epsilon_u/\epsilon_l)$ if $\alpha = 1$. The term L is the total energy radiated between ϵ_l and ϵ_u in the comoving blob frame. Equation (1) simplifies to

$$S(\epsilon; \Omega) = \frac{\mathscr{D}^{3+\alpha} k_\alpha L (1+z)^{1-\alpha} \epsilon^{-\alpha}}{4\pi d_L^2}, \quad \epsilon_l \le \frac{\epsilon(1+z)}{\mathscr{D}} \le \epsilon_u. \quad (2)$$

Let $n(L, \alpha, \Gamma; z) dL\, d\alpha\, d\Gamma$ represent the differential number of randomly oriented sources per unit proper volume that emit a blob with bulk Lorentz factor Γ between Γ and $\Gamma + d\Gamma$, luminosity L between L and $L + dL$, and spectral index α between α and $\alpha + d\alpha$ at epoch z. For a $q_0 = \frac{1}{2}$ cosmology, the number of gamma-ray sources detectable in a full sky survey by a gamma-ray telescope with threshold flux density greater than S_ϵ, is given by

$$N(>S_\epsilon) = \frac{2\pi c}{H_0} \int_{S_\epsilon}^\infty dS_\epsilon^* \int_0^\infty dL \int_{-\infty}^\infty d\alpha \int_1^\infty d\Gamma \int_{-1}^1 d\mu \times \int_0^\infty dz (1+z)^{-13/2} d_L^2\, n(L, \alpha, \Gamma; z) \times \delta S_\epsilon^* - \frac{\mathscr{D}^{3+\alpha} k_\alpha L (1+z)^{1-\alpha} \epsilon^{-\alpha}}{4\pi d_L^2} H\left(\epsilon; \frac{\mathscr{D}\epsilon_l}{1+z}, \frac{\mathscr{D}\epsilon_u}{1+z}\right)\Bigg\} \quad (3)$$

(see, e.g., Weinberg 1972; Dermer 1992), where $H[x; a, b]$ is the Heaviside function with $H[x; a, b] = 1$ if $a \le x \le b$ and $H[x; a, b] = 0$ otherwise. For simplicity, we consider the case $n(L, \alpha, \Gamma; z) = n_0 \delta(L - \bar{L})\delta(\alpha - 1)\delta(\Gamma - \bar{\Gamma})(1+z)^p$, where n_0 is the number of sources per unit volume at the present epoch and the factor $(1+z)^p$ describes the evolution of the sources ($p = 3$ corresponds to constant number of sources per comoving volume).

The threshold flux density S_ϵ can be estimated from Table 2, using the lower photon energy as a measure of the bandwidth. Thus $S_\epsilon \approx 5 \times 10^{-14}$ ergs s^{-1} ϵ^{-1} represents the 100 MeV

threshold for EGRET, and $S_\epsilon \approx 3 \times 10^{-10}$ ergs s^{-1} ϵ^{-1} represents the 100 keV threshold for OSSE. We assume that the range of power-law behavior is sufficiently great that we can approximate the observed spectrum as a power law in the 100 MeV range for EGRET and the 100 keV range for OSSE. What this means is that $\epsilon_l \ll \mathcal{D}\epsilon_{\rm thr}/(1+z) \ll \epsilon_u$, where $\epsilon_{\rm thr}$ is the lower limit of the energy ranges measured by the gamma-ray telescopes. Solving the δ-functions, we obtain the following result for the predicted differential number of sources per unit z:

$$\frac{dN}{dz} = \frac{2\pi c n_0 (1+z)^{p-13/2} d_L^2}{H_0}(1-\mu_s)\,, \tag{4}$$

where

$$\mu_s = \beta_\Gamma^{-1} - (\beta_\Gamma \Gamma)^{-1}\left(\frac{k_1 L}{4\pi d_L^2 \epsilon_{\rm thr} S_\epsilon}\right)^{1/4}. \tag{5}$$

Woltjer (1990) summarizes the data on the space density of various types of AGNs, which range from ~ 1 to 10^4 Gpc^{-3}. We normalize our results by $n_0 = 3.4 \times 10^{-83} n_{\rm Gpc^{-3}}$ cm^{-3}, where $n_{\rm Gpc^{-3}}$ is the density of the sources in units of Gpc^{-3}. Using the EGRET threshold given above with $\epsilon_l = 1$, $\epsilon_u = 10^8$ and $p = 3$, we obtain the results shown in Figure 5. (Values of $\epsilon_l = 20$ and $\epsilon_u > 2 \times 10^4$ are suggested by EGRET observations, but the results are only weakly sensitive to these values.) Figure 5*a* shows the redshift distribution for $\Gamma = 2$, 5, and 10 and blob luminosities of 10^{44}, 10^{45}, and 10^{46} ergs s^{-1}. The redshift distributions extends over a wide range of z and have a qualitatively similar appearance as the redshift distribution of gamma-ray blazars or the FSRQs shown in Figure 2.

The redshift distributions corresponding to isotropic source emission ($\Gamma = 1$) with luminosities $L = 10^{47}$, 10^{48}, and 10^{49} ergs s^{-1} are shown in Figure 5*b*. For $L = 10^{49}$ ergs s^{-1}, the redshift distribution extends to $z > 3$. Although the shape of these distributions is less qualitatively similar to the blazar distributions of Figure 2*b* than the beamed distributions of Figure 5*a*, little information is available about the luminosity distribution of AGNs, particularly at gamma-ray energies (see Chiang et al. 1994). An appropriate luminosity distribution of unbeamed sources could be simply constructed to explain the statistics of blazars with isotropic sources, *provided* that such large luminosities can be realized by supermassive black hole sources. We return to this question in § 5.3.

Conversely, we can ask whether the observed redshift distribution of gamma-ray Seyferts and radio galaxies, shown in Figure 2*a*, require isotropic sources. Again, the uncertainty in the luminosity functions of AGNs makes it possible, using either isotropic source mechanisms or weakly luminous, highly beamed outflows, to reproduce the redshift distribution of gamma-ray Seyferts, as suggested by the inset to Figure 5*b*. We conclude that the question of beaming in gamma-ray Seyferts or blazars cannot be determined from the statistics of these sources.

5.2. *Gamma-Ray Transparency*

We now consider whether gamma-ray transparency arguments (Mattox et al. 1993; Maraschi, Ghisellini, & Celotti 1992; Blandford 1993) require beaming of the gamma-ray emission. According to this argument, one assumes that the gamma-ray source is at rest in the cosmological frame and that the observed gamma-ray variability timescale $\delta t_{\rm obs}$ implies a maximum size scale $R \lesssim c\,\delta t_{\rm obs}/(1+z)$ of the source according to simple light travel time arguments. If the X-rays are produced in the same region as the gamma rays, then the pair production optical depth $\tau_{\gamma-\gamma}$ greatly exceeds unity for sources such as 3C 279 and 1633+382. Relativistic bulk motion of the emitting region reduces the required photon energy density in the source so that it is transparent to 100 MeV–GeV gamma rays. This argument depends critically on the assumption that the X-rays are made in the same region as the gamma rays, which has not been demonstrated through observations of correlated X-ray emission and $E > 100$ MeV gamma-ray emission. If we relax this assumption and consider only the trans-

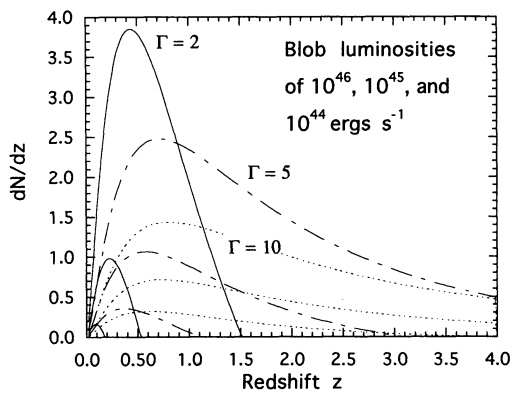

FIG. 5*a*

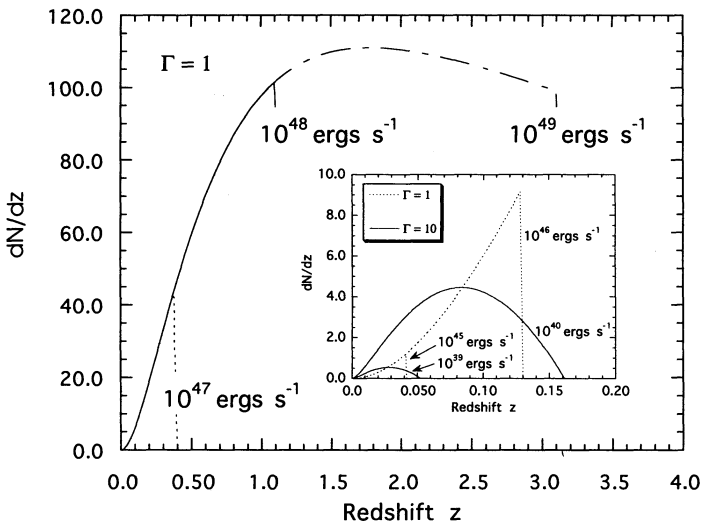

FIG. 5*b*

FIG. 5.—Differential redshift distributions of beamed and isotropic sources detectable with EGRET, where we assume an intrinsic photon spectrum with $s = 2$ over a wide energy range (see text for details of normalization and assumptions), a density of sources in the cosmological frame of 1 per Gpc^{-3}, and no source evolution. (*a*) Redshift distributions of monoluminosity blobs traveling in random directions with bulk Lorentz factors $\Gamma = 2$, 5, and 10. The integrated comoving frame luminosities of the blobs are (from top to bottom) 10^{46}, 10^{45}, and 10^{44} ergs s^{-1}. (*b*) Redshift distributions of isotropically radiating sources with differing luminosities. The maximum redshift for which a source with a given luminosity is detectable is indicated for sources with luminosities of 10^{47}, 10^{48}, and 10^{49} ergs s^{-1}. Note the z^2 volume dependence of the redshift distribution at small redshift. The inset to Fig. 5*b* shows the redshift distribution of weak isotropic sources (*dotted curves*), and weak beamed sources (*solid curves*). The space density of the beamed sources in the inset is 1000 per Gpc^{-3}.

parency of gamma rays to each other, then the gamma-ray transparency argument fails, as we show.

From the formulation of Gould & Schréder (1967), we can write

$$\tau_{\gamma-\gamma}(\epsilon_1) = \int_{x_0}^{x_1} dx' \; -1 \int_{-1}^{1} d\mu (1-\mu) \times \int_{2/\epsilon_1(1-\mu)}^{\infty} d\epsilon \, \sigma_{\gamma-\gamma}(s) n_{\rm ph}(\epsilon, , \mu \, x') \,, \quad (6)$$

where $n_{\rm ph}(\epsilon, \mu; x')d\epsilon \, d\mu$ is the differential number of photons per unit volume at position x' with dimensionless energy ϵ between ϵ and $\epsilon + d\epsilon$ and with direction cosine $\mu = \cos\theta$ between μ and $\mu + d\mu$, where θ is the angle between the directions of photons with energy ϵ and ϵ_1. The invariant $s = 2\epsilon\epsilon_1(1 - \mu)$, so that threshold pair production corresponds to $s = 4$. The expression for the pair-production cross section $\sigma_{\gamma-\gamma}(s)$ is quoted in Gould & Schréder; in the high-energy asymptotic regime $s \gg 1$,

$$\sigma_{\gamma-\gamma}(s) \rightarrow \frac{3\sigma_T}{2s}\left(1 + \frac{4}{s}\right)(\ln s - 1) \,. \quad (7)$$

If we approximate the source of radiation as a homogeneous, quasi-isotropic spherical source of radius R, then the mean photon spectral density $n_{\rm ph}(\epsilon) \cong 3L(\epsilon)/(4\pi R^2 c\epsilon m_e c^2)$ where, as in § 5.1, $L(\epsilon)$ is the spectral luminosity. Denoting the observed photon flux by $\Phi(\epsilon)$ (photons cm^{-2} s^{-1} ϵ^{-1}), equation (2) implies for our assumptions that $L(\epsilon) \cong 4\pi d_L^2 \Phi[\epsilon/(1 + z)]\epsilon m_e c^2/(1 + z)^2$, so that

$$n_{\rm ph}(\epsilon) \cong \frac{3d_L^2}{R^2 c} \frac{\Phi[\epsilon/(1+z)]}{(1+z)^2} \,. \quad (8)$$

Substituting equations (7) and (8) into equation (6) and approximating the typical scattering event by a $\mu = 0$ interaction, we obtain

$$\tau_{\gamma-\gamma}(\epsilon_1) \cong \frac{9d_L^2\sigma_T}{4\epsilon_1 Rc(1+z)^2} \int_{\tilde{s}_{\rm min}(\gg 4)}^{\infty} d\tilde{s} \left(\frac{\ln\tilde{s} - 1}{\tilde{s}}\right) \Phi\left[\frac{\tilde{s}}{2\epsilon_1(1+z)}\right] , \quad (9)$$

where $\tilde{s} = 2\epsilon\epsilon_1$ and $\sigma_{\gamma-\gamma}(\tilde{s}) \rightarrow 3\sigma_T(\ln\tilde{s} - 1)/2\tilde{s}$.

We can write

$$\Phi(\epsilon) = \frac{(s-1)F(\epsilon_l, \epsilon_u)}{\epsilon_l^{1-s} - \epsilon_u^{1-s}} \epsilon^{-s} \,, \quad \epsilon_l \le \epsilon \le \epsilon_u \quad (10)$$

for the photon flux, where $F(\epsilon_l, \epsilon_u)$ is the photon flux integrated between dimensionless photon energies ϵ_l and ϵ_u. To be consistent with the assumption $\tilde{s} \gg 4$, we always consider values of ϵ_l and ϵ_1 such that $2\epsilon_l\epsilon_1(1 + z) \gg 4$. Substituting equation (10) into equation (9) and evaluating the logarithmic term at the lower limit of the integration, we find that

$$\tau_{\gamma-\gamma}(\epsilon_1) \cong \frac{9d_L^2\sigma_T(1 - s^{-1})}{4Rc(1+z)^2} \frac{F(\epsilon_l, \epsilon_u)\ln[0.735\epsilon_l\epsilon_1(1+z)]}{\epsilon_l\epsilon_1[1 - (\epsilon_u/\epsilon_l)^{1-s}]} \,. \quad (11)$$

The first EGRET catalog (Fichtel et al. 1994) lists the integrated photon flux $F(\epsilon_l, \epsilon_u) \equiv 10^{-6}F_{-6}$ in units of 10^{-6} photons cm^{-2} s^{-1} between photon energies 100 MeV and 5 GeV (i.e., $\epsilon_l = 196$ and $\epsilon_u \cong 10^4$). Writing $\epsilon_l = 196e_{100}$ and $\epsilon_1 = 196E_{100}$ to preserve generality, we find that the optical depth for photons with energy $E = 100E_{100}$ MeV, interacting with the measured photon flux that is assumed to be emitted from a homogeneous spherical region with size scale $R \lesssim c\,\delta t_{\rm obs}/(1 + z)$, is given by

$$\tau_{\gamma-\gamma}(E_{100}) \cong \frac{3.0 \times 10^{-3}}{e_{100}E_{100}} \frac{(1 - s^{-1})F_{-6}f^2(z)}{h^2\delta t({\rm days})(1+z)} \times \{1 + 0.098\ln[e_{100}E_{100}(1+z)]\} \,, \quad (12)$$

provided that $\epsilon_1 \equiv E_1/0.511 \gg 2/\epsilon$, where E_1 is the energy in MeV. Here we have defined the luminosity distance $d_L = 2cf(z)/H_0$, where $f(z) = 1 + z - (1 + z)^{1/2}$, appropriate to a $q_0 = \frac{1}{2}$ cosmology.

In Table 4, we list values of the pair production optical depth $\tau_{\gamma-\gamma}(E_1)$ for 100 MeV photons and 1 MeV photons passing through the $E > 100$ MeV emission region inferred from EGRET observations. Here we use values of the $E > 100$ MeV photon fluxes at the time when the emission was midway between the two flux levels defining the most rapid variability timescale (Michelson et al. 1994). As can be seen, EGRET observations *alone* offer no evidence for beaming from gamma-ray transparency arguments. The largest derived value of the pair absorption opacity $\tau_{\gamma-\gamma}(100\ {\rm MeV})$ is only $\sim 6 \times 10^{-4}$ for PKS 0528 + 134. Lower energy observations of variability with COMPTEL have the potential to provide larger values of $\tau_{\gamma-\gamma}$ because the energies are smaller. For example, Collmar et al. (1994) argue that the 3–10 MeV time-variable flux of PKS 0528 + 134 follows the EGRET light curve. If we adopt a 2 day variability timescale for emission at 10 MeV, then this implies that $\tau_{\gamma-\gamma}(10\ {\rm MeV})$ is $\sim 10\%$ for PKS 0528 + 134. Only for X-γ pair production has beaming been claimed to be demon-

TABLE 4

PAIR-PRODUCTION OPTICAL DEPTHS OF GAMMA-RAY AGNs

Source	Δt(days)	s[a]	F_{-6}	z	$f(z)$	$\tau_{\gamma-\gamma}(E_{100} = 1)$	$\tau_{\gamma-\gamma}(E_{100} = 0.01)$
1253 − 055 (3C 279)[b]	2	1.9 ± 0.1	3.0	0.538	0.298	1.3×10^{-4}	6.0×10^{-3}
2251 + 158[c]	4	2.2 ± 0.1	1.0	0.859	0.496	5.7×10^{-5}	3.3×10^{-3}
0235 + 164[d]	<90	2.0 ± 0.2	0.5	0.94	0.55	1.4×10^{-6}	7.8×10^{-5}
0208 − 512[d]	8	1.7 ± 0.1	0.7	1.003	0.587	2.0×10^{-5}	1.1×10^{-3}
1633 + 382[e]	2	1.9 ± 0.1	1.0	1.81	1.13	3.6×10^{-4}	2.0×10^{-2}
0528 + 134[f]	2	2.6 ± 0.1	1.0	2.06	1.31	5.7×10^{-4}	3.3×10^{-2}

[a] Fichtel et al. 1994.
[b] Kniffen et al. 1993.
[c] Hartman et al. 1994.
[d] Michelson et al. 1994.
[e] Mattox et al. 1993.
[f] Hunter et al. 1993a.

strated, and then it must be argued that the observed X-rays originate in the same region as the gamma rays, which may well be false.

The OSSE instrument, however, is sensitive in the range where gamma-ray transparency arguments can be applied without correlated X-ray observations, as is required for EGRET. Recent analysis (McNaron-Brown et al. 1995) of OSSE data for 3C 454.3, CTA 102, and PKS 0528+134 indicates large $\gamma-\gamma$ optical depths for photons with energies detected with OSSE, in which case beaming is implied. There remains the question in this analysis whether the $\gtrsim 1$ MeV photons originate from the same region as the $\lesssim 1$ MeV photons, but the smoothness of the spectrum through this regime makes that assumption more plausible than the arguments for the higher energy observations. In the EGRET analysis, for instance, it is necessary to assume that X-ray photons with energies 4–5 orders of magnitude less than the $\gtrsim 100$ MeV photons detected with EGRET are produced in the same region.

5.3. *Luminosity and Mass Estimates*

If one assumes isotropically emitting sources, then the gamma-ray luminosities of some AGNs such as PKS 0528+134 reach $\sim 10^{49}$ ergs s^{-1}. The implied minimum black hole mass for Eddington-limited accretion in the Thomson regime is well-known: $M_8 \lesssim L_T/(1.26 \times 10^{46}$ ergs s$^{-1})$, where L_T is the bolometric luminosity for emission in the Thomson regime. However, because gamma rays in the EGRET energy range have energies $\epsilon \gg 1$, Klein-Nishina effects on the Compton scattering cross section must be considered when inferring Eddington-limited masses for EGRET sources.

Using the Klein-Nishina cross section, the radiation force exerted through Compton scattering from a point source of isotropic emission with spectral luminosity $L(\epsilon)$ is given by

$$F_C = \frac{\sigma_T}{4\pi r^2 c}\,\hat{r}\int_0^\infty d\epsilon\, L(\epsilon)\kappa(\epsilon)\,, \tag{13a}$$

where

$$\kappa(\epsilon) = \frac{3(1+\epsilon)}{4\epsilon^3(1+2\epsilon)^3}\left[\frac{(1+2\epsilon)^3}{2\epsilon}(\epsilon^2-2\epsilon-3)\ln(1+2\epsilon) + 3 + 17\epsilon + 31\epsilon^2 + 17\epsilon^3 - \frac{10\epsilon^4}{3}\right], \tag{13b}$$

with limiting forms

$$\kappa(\epsilon) \to \begin{cases} 1 - \dfrac{16\epsilon}{5}\,, & \epsilon \ll 1 \\ \dfrac{3}{8\epsilon}\left[\ln(1+2\epsilon) - \dfrac{5}{6}\right] & \epsilon \gg 1 \end{cases} \tag{14}$$

(Pozdnyakov, Sobol', & Sunyaev 1983). In Figure 6 we plot $\kappa(\epsilon)$ along with the limiting expressions given by equation (14).

We approximate the flux by a power-law spectrum given by equation (10). Eddington-limited accretion for a hydrogen plasma implies that $|F_G| = GMm_H/r^2 > |F_C|$. Using the relation between $L(\epsilon)$ and $\Phi(\epsilon)$ preceding equation (8), we obtain an expression for the minimum mass of a black hole, in units of $10^8\ M_\odot$, which is assumed to emit isotropic radiation by steady, Eddington-limited accretion, given by

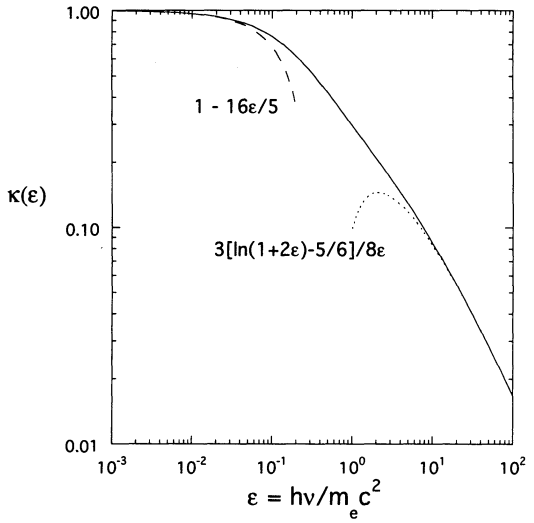

FIG. 6.—The function $\kappa(\epsilon)$ (Pozdnyakov et al. 1983) from eq. (13b), which gives the Compton radiation force through eq. (13a). Also shown are the $\epsilon \ll 1$ and $\epsilon \gg 1$ asymptotes (eqs. [14]).

$$M_8^C \gtrsim \frac{4\pi d_L^2(m_e c^2)(1+z)^{-2}}{1.26\times 10^{46}\ \text{ergs s}^{-1}}\int_{\epsilon_l(1+z)}^{\epsilon_u(1+z)} d\epsilon\,\epsilon\Phi\left(\frac{\epsilon}{1+z}\right)\kappa(\epsilon)\,. \tag{15}$$

The limiting form of equation (15) in the Thomson regime $\epsilon \ll 1$ is

$$M_8^T \gtrsim \frac{4\pi d_L^2(m_e c^2)}{1.26\times 10^{46}\ \text{ergs s}^{-1}}\left(\frac{s-1}{s-2}\right)\left(\frac{\epsilon_l^{2-s}-\epsilon_u^{2-s}}{\epsilon_l^{1-s}-\epsilon_u^{1-s}}\right)F(\epsilon_l,\epsilon_u)\,, \tag{16a}$$

where we keep only the constant term in the Thomson limit of $\kappa(\epsilon)$ in equation (14). In the Klein-Nishina regime, we find

$$M_8^{KN} \gtrsim \frac{3\pi d_L^2(m_e c^2)}{2\cdot 1.26\times 10^{46}\ \text{ergs s}^{-1}}\,\frac{F(\epsilon_l,\epsilon_u)}{1+z}\ln[2\epsilon_l(1+z)]\,, \tag{16b}$$

where we have approximated the logarithmic term in the Klein-Nishina limit of equation (14) by the lower limit of integration.

In Table 5, we list the implied minimum black hole masses for the brightest AGNs observed at gamma-ray energies, under the assumptions of isotropic radiation and Eddington-limited accretion. The Thomson limit expression (16a) is used for the 50–150 keV OSSE measurements. We see that the weak OSSE detection of PKS 0528+134 implies the largest black hole mass, namely $M \gtrsim 6\times 10^9\ M_\odot$. Klein-Nishina corrections to the radiation force in the photon energy range 0.05–0.15 MeV will reduce the implied minimum masses of low-redshift sources by a factor 0.76–0.53, as can be verified from Figure 6. In the case of PKS 0528+134, with $z = 2.08$, the implied minimum black hole mass is reduced from the Thomson result by a factor 0.3–0.5, so that the largest minimum black hole mass implied from OSSE observations is therefore $\approx 2.5\times 10^9\ M_\odot$. A value of $\approx 7\times 10^9\ M_\odot$ is obtained for PKS 0528+134, however, by McNaron-Brown et al. (1995) by considering the full OSSE bandwidth, including Klein-Nishina corrections to the radiation force.

TABLE 5

MINIMUM BLACK HOLE MASSES OF GAMMA-RAY AGNs IMPLIED BY EDDINGTON-LIMITED ACCRETION

Source	z	s(OSSE)[a]	F(OSSE)[a,b]	F(EGRET)[c]	$M_{8,\min}^{\rm OSSE}$	$M_{8,\min}^{\rm EGRET}$
3C 273	0.158	1.69 ± 0.05 (6/91)	1.734 ± 0.048	0.21 ± 0.04 (6/91)	0.96	0.93
3C 279	0.538	2.29 ± 0.32 (9/91)	0.622 ± 0.065	2.7 ± 0.1 (6/91)	4.3	0.19
CTA 102	1.037	1.13 ± 0.32 (3/94)	0.398 ± 0.095	0.25 ± 0.05 (1/92)	13	0.057
1633+382.....	1.81	...	...	1.00 ± 0.08 (9/91)	...	0.11
0528+134.....	2.06	1.60 ± 0.31 (4/94)	0.446 ± 0.053	0.81 ± 0.07 (5/91)	64	0.39

[a] W. N. Johnson, private communication 1994; McNaron-Brown et al. 1995.
[b] Units of 10^{-3} photons cm^{-2} s^{-1} in range 0.05–0.15 MeV.
[c] Fichtel et al. 1994; units of 10^{-6} photons cm^{-2} s^{-1} in range 100 MeV–5 GeV.

Because $E > 100$ MeV gamma-ray emission measured by EGRET is well into the Klein-Nishina regime, the values for the inferred minimum black hole masses are less than those implied by the OSSE measurements, and are in the range 10^6–10^8 $M_\odot$. In spite of the apparently enormous luminosities if the $E > 100$ MeV emission is isotropically radiated, we see that the required black hole masses from the EGRET measurements are not exceptionally great. We speculate that sources in nature can accrete at rates much greater than the Thomson Eddington luminosity if they radiate photons in the gamma-ray regime. If such sources exist, then black hole fueling and the evolutionary behavior of black hole masses can occur much more rapidly than calculated on the basis of Thomson Eddington-limited arguments for accretion (e.g., Rees 1984).

5.4. *Time Variability and Beaming Constraints*

Arguments for beaming can also be made on the basis of the temporal variability of the source luminosity. Such arguments have been developed in two directions, yet yield very similar results. In one version, due to Elliot & Shapiro (1974), it is noted that the Thomson Eddington limit yields a lower limit on the black hole mass M given by equation (16a), which we can write as $M_8 \gtrsim 10^2\ L_{48}$, where $10^{48} L_{48}$ ergs s^{-1} is the (assumed) isotropic source luminosity at $\epsilon \ll 1$. From simple light travel-time arguments, variations of luminosity by a factor ~ 2 on the timescale $\delta t_{\rm obs}$ imply that the characteristic size R of the emitting region is given by $R \lesssim c\,\delta t_{\rm obs}/(1+z)$. Since this minimum size scale is roughly the Schwarzschild radius, we find that $M_8 \lesssim 10^{-3}\,\delta t_{\rm obs}(s)/(1+z)$. Combining these yields an upper and lower bound upon M, so that observations showing that $L_{48}/\delta t_{\rm obs}({\rm days}) \gtrsim 1/(1+z)$ provide evidence in favor of beaming. Generalization of this result to a Schwarzschild metric with zero-stress boundary condition at the innermost stable radius $R_I = 6R_g$, gives $L_{48}/\delta t_{\rm obs}({\rm days}) \lesssim 2.25(1-6\rho^{-1})/\rho(1+z)$ for isotropically emitting sources, where $\rho = R/R_I \geq 1$ (Dermer 1994).

The second version of this argument, due originally to Cavallo & Rees (1978) and applied to AGNs by Fabian (1979; see also Fabian 1992), is based on the idea that the rate of change of luminosity is increased by efficient conversion of rest mass energy into radiation, but is decreased due to the diffusive escape of photons through the matter that is the source of the energy. The implied limit is $L_{48}/\delta t_{\rm obs}({\rm days}) \lesssim 1.7\eta_{0.1}/(1+z)$ (Fabian 1979), where $\eta_{0.1}$ is the conversion efficiency of rest-mass energy into radiation in units of 0.1. *Ginga* observations (Makino et al. 1989) of luminous X-ray emission from 3C 279, varying by 20% on timescales of 45 minutes apparently violate this limit and therefore imply beaming.

Both of these arguments assume that photons interact with matter in the Thomson regime. It is straightforward to generalize the results to the Klein-Nishina regime. Without presenting the detailed formulas, it is sufficient to point out that the limits quoted above must be multiplied by a factor $\approx 8\bar{\epsilon}/3\ln\bar{\epsilon}$ (see eq. [14]), where $\bar{\epsilon} \gg 1$ is the photon energy where the bulk of the luminosity is radiated (i.e., the peak of the νF_ν spectrum). If $\bar{\epsilon} \approx 200$, corresponding to 100 MeV gamma rays, then the Shapiro-Elliot relation and the efficiency limits of Fabian are increased by a factor $\approx 10^2$. The most luminous and rapidly variable EGRET blazars, namely 3C 279 (Kniffen et al. 1993), 1633+382 (Mattox et al. 1993), and PKS 0528+134 (Hunter et al. 1993a) have measured values of $L_{48} = 19$, 10, and 9, respectively (Fichtel et al. 1994). Each has been observed to vary by a factor ≈ 2 on a 2 day timescale. We obtain values $L_{48}(1+z)/\delta t_{\rm obs}({\rm days}) \approx 15$ for all three cases. Given the correction factor of ≈ 100 for emission in the EGRET range, we conclude that present EGRET gamma-ray observations do not require beaming using these arguments.

OSSE observations of blazars also, at present, do not strongly violate the limits of Elliot & Shapiro and Fabian. Table 5 lists the inferred minimum masses measured with OSSE in the 50–150 keV range. From these values of M_8 we obtain L_{48}, since we have assumed Eddington-limited luminosities in the Thomson limit. Hence $L_{48} = 0.0126 M_8$, so that $L_{48} \cong 0.8$ for PKS 0528+134. There is weak OSSE evidence ($\cong 2.5\ \sigma$) for factor of two variability on a 3 day timescale (McNaron-Brown et al. 1995), and the more detailed analysis given in that paper gives mass estimates nearly in conflict with the Elliot-Shapiro relation. But more sensitive data of AGNs are required to demonstrate a strong conflict in order to argue convincingly for beaming from the Elliot-Shapiro relation or the efficiency limit of Fabian.

6. DISCUSSION AND SUMMARY

As of the end of 1994, at least 65 AGNs have been detected at energies $\gtrsim 20$ keV, more than 3 times the number known prior to the launch of *Compton* in 1991 April. We have shown via several lines of evidence that, with a few notable exceptions, gamma-ray AGNs fall into two distinct classes. One class consists of sources with gamma-ray spectra which soften or exponentially cut off between ~ 100 keV and several MeV, and which are associated primarily with AGNs identified as Seyferts in lower energy wavelength ranges. The other class consists of sources with hard gamma-ray spectra extending to 10 GeV or more, and which exhibit blazar properties at other wavelength ranges. Interpretation of previous radio through X-ray AGN data indicate that the nuclear emission from Seyfert AGNs and radio-quiet QSOs is consistent with iso-

tropically radiating sources, although geometrical orientation and obscuration effects play an important role in differences between Seyfert classes. By contrast, Doppler-boosted jet emission is thought to be responsible for blazar-type characteristics (see the reviews cited in the Introduction). We have cataloged the new gamma-ray data and demonstrate the existence of two distinct classes of gamma-ray AGNs.

The gamma-ray Seyfert class consists primarily of classical Seyfert 1's, but also includes a few Seyfert 2's and several radio galaxies also classified as Seyferts. They are nearby AGNs with $z \lesssim 0.06$ and are detected with hard X-ray and low-energy gamma-ray instruments, but not above ≈ 1 MeV. The new discovery by *Granat*/SIGMA and OSSE, coupled with COMPTEL and EGRET upper limits, is that the spectra exponentially cut off or soften above ~ 50–100 keV, consistent with emission from a hot thermal plasma. Combined with the implied small-scale size of the emission region, this suggests that the gamma rays are produced in the inner accretion disk near the black hole.

Supporting evidence for quasi-isotropic nuclear radiation from these sources is the similarity between the gamma-ray spectral shapes for Seyferts and for galactic black holes (see also Inoue 1994). This is illustrated in Figure 7 which compares the spectrum of NGC 4151 with the low-state spectrum of the black hole candidate Cygnus X-1. The Cyg X-1 system consists of a compact object of mass $\sim 6\ M_\odot$ in orbit around a blue supergiant. Both spectra are well fitted with thermal Compton scattering models with $kT = 30$–40 keV (Maisack et al. 1993; Sunyaev & Trümper 1979). The luminosity of Cyg X-1 is $\sim 3 \times 10^{37}$ ergs s^{-1} which is $\sim 0.04 L_{\rm Edd}$ for a $6\ M_\odot$ black hole. By analogy, if the $\sim 2 \times 10^{43}$ ergs s^{-1} for NGC 4151 corresponds to $\sim 0.04 L_{\rm Edd}$, then the black hole mass would be $\sim 10^6$–$10^7\ M_\odot$.

The gamma-ray blazars are a new class of gamma-ray AGNs discovered with EGRET. They consist of BL Lac objects and FSRQs with redshifts ranging from $z = 0.031$ to $z \approx 2.3$. They are detected at $E > 100$ MeV, but are not strongly detected with lower energy gamma-ray instruments. This implies that their spectra soften between the soft and medium-energy gamma ray regimes, in which case the spectra of many of the sources fall below the sensitivities of the current generation of soft gamma-ray telescopes. Above ~ 10 MeV, a power law with photon index $s \approx 2$ represents the mean gamma-ray blazar spectrum. The spectra are hard and nonthermal in the range 100 MeV–10 GeV. The nearest BL Lac object, Mrk 421, is detected at TeV energies with a flux that falls on the extrapolation of the $s = 2$ power-law spectrum from lower energies.

The two classes exhibit clear-cut differences between their redshift and luminosity distributions and gamma-ray spectral characteristics. Because one class is associated with radio-quiet Seyferts and radio galaxies, and the other with sources which display blazar properties, we could expect that these differences

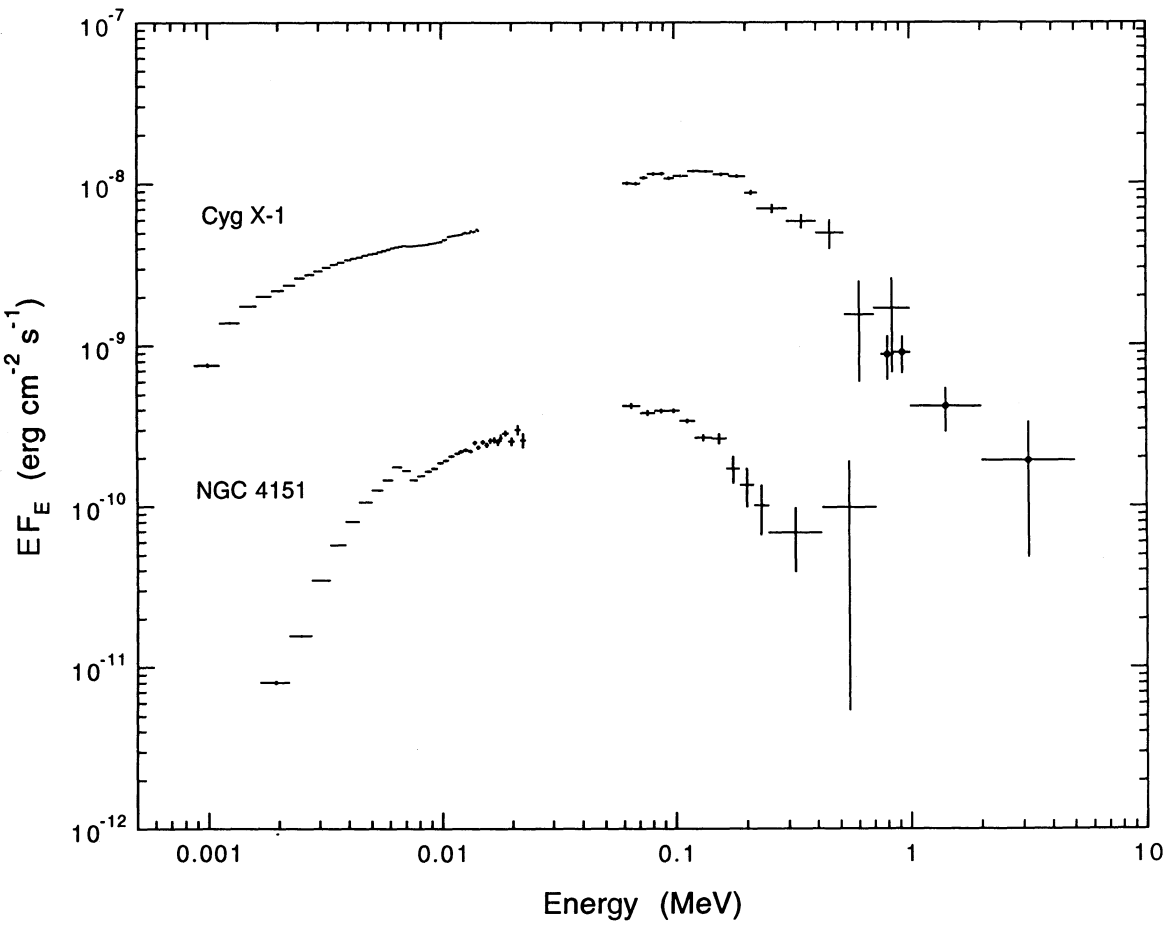

FIG. 7.—Comparison of the power spectral fluxes of NGC 4151 and Cygnus X-1. The Cyg X-1 data are from Bałucinska & Hasinger (1991), Grabelsky et al. (1993), and McConnell et al. (1994), and the NGC 4151 data are from Yaqoob et al. (1993) and Maisack et al. (1993).

originate in their respective emission mechanisms, particularly in view of results and interpretations of AGNs at lower energies. In particular, we expect that the gamma-ray blazar class would display properties related to collimated, relativistic outflow and beamed, Doppler-boosted emission (Blandford & Rees 1978). The gamma-ray observations do not provide, however, conclusive evidence for beaming on the basis of the statistics and luminosity distributions of gamma-ray AGNs, since luminosity functions and space densities of these sources are poorly known. The enormous luminosities measured by EGRET, even if one assumes that the gamma-ray emission from blazars is emitted isotropically, do not require unacceptably large black hole masses, because the Eddington luminosity limit is weakened when radiation is produced in the Klein-Nishina regime. OSSE observations are beginning to indicate, however, that masses $\gg 10^9\ M_\odot$ would be required for isotropic emission in some cases. Measured gamma-ray variability timescales are also not yet sufficiently short to argue in favor of beaming through the Elliot-Shapiro relation (1974) or the efficiency limits of Fabian (1979). Even the association of gamma-ray blazars with superluminal sources is not convincing in arguing for beaming in the gamma-ray blazar class: although $10(\pm 1)$ out of 44 EGRET AGNs have measured superluminal motions, two and perhaps three out of the five radio galaxies have displayed superluminal motions. Only gamma-ray transparency arguments based on OSSE data for PKS 0528+134, CTA 102, and 3C 454.3 (McNaron-Brown et al. 1995) provide, at present, evidence for beaming from the gamma-ray data alone.

In conclusion, we have identified two classes of gamma-ray AGN on the basis of their distinctive spectra, redshift, and luminosity distributions. Even though one class is associated with radio-quiet Seyferts and radio galaxies, and the other is associated with blazars, the evidence for beamed emission as the origin of the differences in the latter class from the gamma-ray data alone is weak. If the gamma-ray emission is produced isotropically at the emission site, however, then geometrical obscuration would be necessary to explain the fact that only flat-spectrum, compact core radio quasars are detected at $E > 100$ MeV energies. More sensitive OSSE observations of AGNs, or correlated X-ray and EGRET gamma-ray observations are required to strengthen arguments for beaming from the gamma-ray data. Superluminal observations probably still provide the most compelling evidence for bulk relativistic motion in blazars. Identifying the processes that are responsible for the two classes of AGNs detected at gamma-ray energies will provide important knowledge about the fueling, acceleration, and radiation processes which operate in sources powered by accretion.

We acknowledge the OSSE team for discussions about the OSSE data, and thank W. N. Johnson for providing the NGC 4151 data, K. McNaron-Brown for early access to blazar data, and R. L. Kinzer for providing the Cen A data. We thank T. Yaqoob and the *Ginga* team for providing the NGC 4151 X-ray data, F. Makino and the *Ginga* team for the 3C 279 X-ray data, and G. Madejski for providing the IC 4329A data. We also thank R. C. Hartman, R. C. Lamb, J. R. Mattox, and J. G. Skibo for comments and discussions, the anonymous referee for valuable suggestions, and K. Pollock for assistance. C. D. acknowledges partial support for this work under NASA grant DPR S-14643-F.

REFERENCES

Antonucci, R. 1993, ARA&A, 31, 473
Auriemma, G., et al. 1978, ApJ, 221, L7
Ayani, K., Maehara, H. 1991, PASJ, 43, L1
Bailey, J., Sparks, W. B., Hough, J. H., & Axon, D. J. 1986, Nature, 322, 150
Baity, W. A., Jones, T. W., Wheaton, W. A., & Peterson, L. E. 1975, ApJ, 199, L5
Baity, W. A., et al. 1981, ApJ, 244, 429
Baity, W. A., Mushotzky, R. F., Worrall, D. M., Rothschild, R. E., Tennant, A. F., & Primini, F. A. 1984, ApJ, 279, 555
Bałucinska, M., & Hasinger, G. 1991, A&A, 241, 439
Bassani, L., & Dean, A. J. 1983, Space Sci. Rev., 35, 367
Bassani, L., et al. 1986, ApJ, 311, 623
———. 1991, Proc. 22d Int. Cosmic Ray Conf., Dublin, 1, 173
———. 1992, ApJ, 396, 504
Beall, J. H., Rose, W. K., Dennis, B. R., Crannell, C. J., Dolan, J. F., Frost, K. J., & Orwig, L. E. 1981, ApJ, 247, 458
Begelman, M. C., Blandford, R. D., & Rees, M. J. 1984, Rev. Mod. Phys., 56, 255
Bertsch, D. L., et al. 1993, ApJ, 405, L21
Bezler, M., et al. 1984, A&A, 136, 351
Bhattacharya, D., et al. 1994, ApJ, 437, 173
Bignami, G. F., Fichtel, C. E., Hartman, R. C., & Thompson, D. J. 1979, ApJ, 232, 649
Blandford, R. D. 1993, in Compton Gamma-Ray Observatory, ed. M. Friedlander, N. Gehrels, & D. J. Macomb (New York: AIP), 533
Blandford, R. D., & Königl, A. 1979, ApJ, 232, 34
Blandford, R. D., & Rees, M. J. 1978, in Pittsburgh Conf. on BL Lac Objects, ed. A. M. Wolfe (Pittsburgh: Univ. Pittsburgh Press), 328
Bloemen, H., et al. 1995, A&A, in press
Blom, J. J., et al. 1994, in The Second Compton Symposium, ed. C. E. Fichtel, N. Gehrels, & J. P. Norris (New York: AIP), 644
———. 1995, A&A, in press
Bolton, J. G., et al. 1979, Aust. J. Physics, Astrophys. Suppl., No. 46
Bond, I. A., et al. 1990, Proc. 21st Int. Cosmic Ray Conf., Adelaide, 2, 271
Brazier, K. T. S., et al. 1990, Proc. 21st Int. Cosmic Ray Conf., Adelaide, 2, 288
Bregman, J. N. 1990, A&A Rev., 2, 125
Cameron, R. A., et al. 1993, in Compton Gamma-Ray Observatory, ed. M. Friedlander, N. Gehrels, & D. J. Macomb (New York: AIP), 478
Cavallo, G., & Rees, M. J. 1978, MNRAS, 183, 359
Chiang, J., et al. 1994, in The Second Compton Symposium, ed. C. E. Fichtel, N. Gehrels, & J. P. Norris (New York: AIP), 654
Coe, M. J., Bassani, L., Engel, A. R., & Quenby, J. J. 1981, MNRAS, 195, 241
Collmar, W., et al. 1993, in Compton Gamma-Ray Observatory, ed. M. Friedlander, N. Gehrels, & D. J. Macomb (New York: AIP), 483
———. 1994, in The Second Compton Symposium, ed. C. E. Fichtel, N. Gehrels, & J. P. Norris (New York: AIP), 659
Damle, S. V., Kunte, P. K., Naranan, S., Sreekantan, B. V., & Venkatesan, D. 1987, A&A, 186, L20
Dean, A. J., et al. 1990, ApJ, 349, 41
De Jager, O. C., Stecker, F. W., & Salamon, M. H. 1994, Nature, 369, 294
Dermer, C. D. 1992, Phys. Rev. Lett., 68, 1799
———. 1994, in Proc. Moriond Workshop on Particle Astrophysics, Atomic Physics, and Gravitation, VIllars sur Ollon, Switzerland, January 22–29, 1994, ed. J. Tran Thanh Van (Gif-sur-Yvette: Editions Frontières), 47
Dermer, C. D., & Schlickeiser, R. 1992, Science, 257, 1642
———. 1994, ApJS, 90, 945
Dingus, B. L., et al. 1993, IAU Circ. No. 5690
Ebneter, K., & Balick, B. 1983, PASP, 95, 675
Elliot, J. L., & Shapiro, S. L. 1974, ApJ, 192, L3
Fabian, A. C. 1979, Proc. R. Soc. Lond. A, 366, 449
———. 1992, in Testing the AGN Paradigm, ed. S. S. Holt, S. G. Neff, & C. M. Urry (New York: AIP), 657
Fabian, A. C., Nandra, K., Celotti, A., Rees, M. J., Grove, J. E., & Johnson, W. N. 1993, ApJ, 416, L57
Fennell, S., et al. 1993, in Compton Gamma-Ray Observatory, ed. M. Friedlander, N. Gehrels, & D. J. Macomb (New York: AIP), 508
Fichtel, C. E. 1993, Ann. NY Acad. Sci., 688 (Texas/PASCOS '92), ed. C. W. Akerlof & M. A. Srednicki), 136
Fichtel, C. E., et al. 1994, ApJS, 94, 551
Fiore, F., Perola, G. C., Matsuoka, M., Yamauchi, M., & Piro, L. 1992, A&A, 262, 37
Frontera, F., Fuligni, F., Morelli, E., & Ventura, G. 1979, ApJ, 234, 477
Gehrels, N., & Cheung, C. 1992, in Testing the AGN Paradigm, ed. S. S. Holt, S. G. Neff, & C. M. Urry (New York: AIP), 348
Gehrels, N., Cline, T. L., Teegarden, B. J., Paciesas, W. S., Tueller, J., Durouchoux, P., & Hameury, J. M. 1984, ApJ, 278, 112
Giuricin, G., Mardirossian, F., Mezzetti, M., & Bertotti, G. 1990, ApJS, 72, 551
Gould, R. J., & Schréder, G. P. 1967, Phys. Rev., 155, 1404

Grabelsky, D. A., et al. 1993, in Compton Gamma-Ray Observatory, ed. M. Friedlander, N. Gehrels, & D. J. Macomb (New York: AIP), 345
Grindlay, J. E. 1993, A&AS, 97, 113
Grindlay, J. E., Helmken, H. F., Brown, R. H., Davis, J., & Allen, L. R. 1975, ApJ, 197, L9
Hall, R. D., Meegan, C. A., Walraven, G. D., Djuth, F. T., & Haymes, R. C. 1976, ApJ, 210, 631
Hartman, R. C., et al. 1992a, ApJ, 385, L1
———. 1992b, IAU Circ., No. 5519
———. 1993, ApJ, 407, L41
———. 1994, in *GRO-Granat* School, Les Houches, in press
Hawarden, T. G., Sandell, G., Matthews, H. E., Friberg, P., Watt, G. D., & Smith, P. A. 1993, MNRAS, 260, 844
Hermsen, W., et al. 1993, A&AS, 97, 97
Herterich, K. 1974, Nature, 250, 311
Hunter, S. D., et al. 1993a, ApJ, 409, 134
———. 1993b, A&A, 272, 59
Hunter, S. D., Digel, S. W., DeGeus, E. J., & Kanbach, G. 1994, ApJ, 436, 216
Hyland, G. B., Fenton, A. G., & Humble, J. E. 1990, Proc. Int. Cosmic Ray Conf., Adelaide, 2, 270
Impey, C. 1987, in Superluminal Radio Sources, ed. J. A. Zensus & T. J. Pearson (New York: Cambridge Univ. Press), 233
Inoue, H. 1994, in IAU Symp. 159, Active Galactic Nuclei across the Electromagnetic Spectrum, ed. T. Courvoisier & A. Blecha (Dordrecht: Kluwer), 73
Jelley, T. V. 1966, Nature, 211, 472
Johnson, W. N., et al. 1994, in The Second Compton Symposium, ed. C. E. Fichtel, N. Gehrels, & J. P. Norris (New York: AIP), 515
———. 1995, ApJ, 445, 000
Jourdain, E., et al. 1992a, A&A, 256, L38
Jourdain, E., et al. 1992b, ApJ, 395, L69
Jourdain, E., et al. 1993, ApJ, 412, 586
Kerrick, A. D., et al. 1994, IAU Circ., No. 5996
Kerrick, A. D., et al. 1993, Proc. 23rd Intl. Cosmic Ray Conf., Calgary, 1, 408
Kinzer, R. L., et al. 1994, in The Second Compton Symposium, ed. C. E. Fichtel, N. Gehrels, & J. P. Norris (New York: AIP), 531
———. 1995, ApJ, in press
Kniffen, D. A., et al. 1993, ApJ, 411, 133
Kurfess, J. D. 1994, in IAU Symp. 159, Active Galactic Nuclei across the Electromagnetic Spectrum, ed. T. Courvoisier & A. Blecha (Dordrecht: Kluwer), 39
Lawrence, A. 1987, PASP, 99, 309
Lichti, G. G., et al. 1994, in The Second Compton Symposium, ed. C. E. Fichtel, N. Gehrels, & J. P. Norris (New York: AIP), 611
———. 1995, A&A, in press
Lightman, A. P., & Zdziarski, A. A. 1987, ApJ, 319, 643
Lin, Y. C., et al. 1992, ApJ, 401, L61
———. 1993, ApJ, 416, L53
———. 1994, in The Second Compton Symposium, ed. C. E. Fichtel, N. Gehrels, & J. P. Norris (New York: AIP), 582
———. 1995, ApJ, 442, 96
Madejski, G. M., et al. 1995, ApJ, 438, 672
Madejski, G. M., Done, C., Turner, T. J., Mushotzky, R. F., Serlemitsos, P., Fiore, F., Sikora, M., & Begelman, M. C. 1993, Nature, 365, 626
Maisack, M., et al. 1992, A&A, 262, 433
———. 1993, ApJ, 407, L61
———. 1994, in The Second Compton Symposium, ed. C. E. Fichtel, N. Gehrels, & J. P. Norris (New York: AIP), 556
Makino, F., et al. 1987, ApJ, 313, 662
———. 1989, ApJ, 347, L9
———. 1993, in Frontiers of Neutrino Astrophysics, ed. Y. Suzuki & K. Nakamura (Tokyo: Universal Press, Inc.), 425
Malaguti, G., Bassani, L., & Caroli, E. 1994, ApJS, 94, 517
Maraschi, L., Ghisellini, G., & Celotti, A. 1992, ApJ, 397, L5
Marscher, A. P., & Bloom, S. D. 1994, in The Second Compton Symposium, ed. C. E. Fichtel, N. Gehrels, & J. P. Norris (New York: AIP), 573
Matt, G., et al. 1990, ApJ, 355, 468
Mattox, J. R., et al. 1993, ApJ, 410, 609
McConnell, M., et al. 1994, ApJ, 424, 933
McNaron-Brown, K., et al. 1994, in The Second Compton Symposium, ed. C. E. Fichtel, N. Gehrels, & J. P. Norris (New York: AIP), 587
———. 1995, ApJ, submitted
Meier, D. L., et al. 1989, AJ, 98, 27
Michelson, P. F., et al. 1992, IAU Circ., No. 5470
———. 1994, in The Second Compton Symposium, ed. C. E. Fichtel, N. Gehrels, & J. P. Norris (New York: AIP), 602
Mohanty, G., et al. 1993, in Proc. Int'l. Cosmic Ray Conf., Calgary, Canada, 1, 440
Morini, M., Anselmo, F., & Molteni, D. 1989, ApJ, 347, 750
Mushotzky, R. F., Baity, W. A., & Peterson, L. E. 1977, ApJ, 212, 22
Mushotzky, R. F., Baity, W. A., Wheaton, W. A., & Peterson, L. E. 1976, ApJ, 206, L45
Mushotzky, R. F., Serlemitsos, P. J., Becker, R. H., Boldt, E. A., & Holt, S. S. 1978, ApJ, 220, 790
Nandra, K., & Pounds, K. A. 1994, MNRAS, 268, 405
Nolan, P. L., et al. 1993, ApJ, 409, 697
Odenwald, S., Gehrels, N., & Howard, S. 1994, in IAU Symp. 159, Active Galactic Nuclei across the Electromagnetic Spectrum, ed. T. Courvoisier & A. Blecha (Dordrecht: Kluwer), 323
Ohashi, T., et al. 1989, Proc. 23d ESLAB Symposium, ed. N. White (Noordwijk: ESA), 837
Osako, C. Y., et al. 1995, ApJ, 438, L25
Paciesas, W. S., Mushotzky, R. F., & Pelling, R. M. 1977, MNRAS, 178, 23P
Paciesas, W. S., et al. 1993a, in Compton Gamma-Ray Observatory, ed. M. Friedlander, N. Gehrels, & D. J. Macomb (New York: AIP), 473
———. 1994, in The Second Compton Symposium, ed. C. E. Fichtel, N. Gehrels, & J. P. Norris (New York: AIP), 674
———. 1993b, A&AS, 97, 253
Paul, J. 1994, in *GRO-Granat* School, Les Houches, in press
Perotti, F., et al. 1981a, ApJ, 247, L63
———. 1981b, Nature, 292, 133
———. 1991, ApJ, 373, 75
Pietsch, W., Reppin, C., Trümper, J., Voges, W., Lewin, W., Kendziorra, E., & Stauber, R. 1981, A&A, 94, 234
Piro, L., Yamauchi, M., & Matsuoka, M. 1990, ApJ, 360, L35
Pohl, M., et al. 1995, A&A, in press
Porcas, R. W. 1987, in Superluminal Radio Sources, ed. J. A. Zensus & T. J. Pearson (New York: Cambridge Univ. Press), 12
Pozdnyakov, L. A., Sobol', J. M., & Sunyaev, R. A. 1983, A&SS Rev., 2, 189
Primini, F. A., et al. 1979, Nature, 278, 234
Punch, M., et al. 1992, Nature, 358, 477
Ramaty, R., & Lingenfelter, R. E. 1982, Ann. Rev. Nucl. Part. Sci., 32, 235
Rees, M. J. 1984, ARA&A, 22, 471
Rothschild, R. E., Baity, W. A., Mushotzky, R. F., Wheaton, W. A., & Peterson, L. E. 1979, in X-Ray Astronomy, ed. W. A. Baity & L. E. Peterson (New York: Pergamon), 369
Rothschild, R. E., Mushotzky, R. F., Baity, W. A., Gruber, D. E., Matteson, J. L., & Peterson, L. E. 1983, ApJ, 269, 423
Schachter, J. F., & Elvis, M. 1994, in The Second Compton Symposium, ed. C. E. Fichtel, N. Gehrels, & J. P. Norris (New York: AIP), 679
Schönfelder, V. 1994, ApJS, 92, 593
Schubnell, M., et al. 1994, in The Second Compton Symposium, ed. C. E. Fichtel, N. Gehrels, & J. P. Norris (New York: AIP), 597
Skibo, J. G., Dermer, C. D., & Kinzer, R. L. 1994, ApJ, 426, L23
Stecker, F. W., de Jager, O. C., & Salamon, M. H. 1992, ApJ, 390, L49
Sunyaev, R., & Titarchuk, L. 1980, A&A, 86, 121
Sunyaev, R., & Trümper, J. 1979, Nature, 279, 506
Swanenburg, B. N., et al. 1978, Nature, 275, 298
Thompson, D. J., et al. 1992, BAAS, 24, 1155
———. 1993a, ApJ, 410, 87
———. 1993b, ApJ, 415, L13
Titarchuk, L., & Mastichiadis, A. 1994, ApJ, 433, L33
Turner, T. J., & Pounds, K. 1989, MNRAS, 240, 883
Ubertini, P., Bazzano, A., Cocchi, M., LaPadula, C., & Sood, R. 1993, A&AS, 97, 105
Ubertini, P., Bazzano, A., LaPadula, C., Polcaro, V. F., & Manchanda, R. K. 1984, ApJ, 284, 54
Urry, C. M., Maraschi, L., & Phinney, E. S. 1991, Comments Astrophys. Space Phys., 15, 111
Vermeulen, R. C., & Cohen, M. H. 1994, ApJ, 430, 467
von Ballmoos, P., Diehl, R., & Schönfelder, V. 1987, ApJ, 312, 134
von Montigny, C., et al. 1993, A&AS, 97, 101
———. 1995, ApJ, 440, 525
Walker, R. C., Benson, J. M., & Unwin, S. C. 1987, in Superluminal Radio Sources, ed. J. A. Zensus & T. J. Pearson (New York: Cambridge Univ. Press), 48
Wall, J. V., & Peacock, J. A. 1985, MNRAS, 216, 173
Weinberg, S. 1972, Gravitation and Cosmology: Principles and Applications of the General Theory of Relativity (New York: Wiley), 454
Williams, O. R., et al. 1995, A&A, in press
Woltjer, L. 1990, Active Galactic Nuclei (New York: Springer), 6
Yaqoob, T., Warwick, R. S., Makino, F., Otani, C., Sokoloski, J. L., Bond, I. A., & Yamauchi, M. 1993, MNRAS, 262, 435
Zdziarski, A. A. 1994, in The Second Compton Symposium, ed. C. E. Fichtel, N. Gehrels, & J. P. Norris (New York: AIP), 525
Zdziarski, A. A., Ghisellini, G., George, I. M., Svensson, R., Fabian, A. C., & Done, C. 1990, ApJ, 363, L1
Zdziarski, A. A., Johnson, W. N., Done, C., Smith, D., & McNaron-Brown, K. 1995, ApJ, 438, L63
Zdziarski, A. A., Lightman, A. P., & Maciołek-Niedźwiecki, A. 1993, ApJ, 414, L93

Note added in proof.—In addition to the sources listed in Table 1, two other AGNs have recently been detected in the gamma-ray band: NGC 4507, a Seyfert 2 galaxy detected with *OSSE* (Bassani, L., et al., ApJ, in press [1995]), and 0954+658, a BL Lac object detected with EGRET (Mukherjee, R., et al., in preparation [1995]).